GLOBAL BIOGEOCHEMICAL CYCLES, VOL. 12, NO. 1, PAGES 141–163, MARCH 1998

# Seasonal variations in the atmospheric $O_2/N_2$ ratio in relation to the kinetics of air-sea gas exchange

Ralph F. Keeling,[1] Britton B. Stephens,[1] Raymond G. Najjar,[2] Scott C. Doney,[3] David Archer,[4] and Martin Heimann[5]

**Abstract.** Observations of seasonal variations in the atmospheric $O_2/N_2$ ratio are reported at nine baseline sites in the northern and southern hemispheres. Concurrent $CO_2$ measurements are used to correct for the effects of land biotic exchanges of $O_2$ on the $O_2/N_2$ cycles thus allowing the residual component of the cycles due to oceanic exchanges of $O_2$ and $N_2$ to be calculated. The residual oceanic cycles in the northern hemisphere are nearly diametrically out of phase with the cycles in the southern hemisphere. The maxima in both hemispheres occur in summer. In both hemispheres, the middle-latitude sea level stations show the cycles with largest amplitudes and earliest phasing. Somewhat smaller amplitudes are observed at the high-latitude stations, and much smaller amplitudes are observed at the tropical stations. A model for simulating the oceanic component of the atmospheric $O_2/N_2$ cycles is presented consisting of the TM2 atmospheric tracer transport model [*Heimann*, 1995] driven at the lower boundary by $O_2$ fluxes derived from observed $O_2$ saturation anomalies in surface waters and by $N_2$ fluxes derived from the net air-sea heat flux. The model is optimized to fit the observed atmospheric $O_2/N_2$ cycles by adjusting the air-sea gas-exchange velocity, which relates $O_2$ anomaly to $O_2$ flux. The optimum fit corresponds to spatially and temporally averaged exchange velocities of 24±6 cm/hr for the oceans north of 31°N and 29±12 cm/hr for the oceans south of 31°S. These velocities agree to within the uncertainties with the gas-exchange velocities expected from the *Wanninkhof* [1992] formulation of the air-sea gas-exchange velocity combined with European Centre for Medium-Range Weather Forecasts winds [*Gibson et al.*, 1997] but are larger than the exchange velocities expected from the *Liss and Merlivat* [1986] relation using the same winds. The results imply that the gas-exchange velocity for $O_2$, like that of $CO_2$, may be enhanced in the open ocean by processes that were not systematically accounted for in the experiments used to derive the Liss and Merlivat relation.

## 1. Introduction

A prominent feature evident in measurements of the atmospheric $O_2/N_2$ ratio at stations in both the northern and southern hemispheres is a quasi-regular seasonal cycle [*Keeling and Shertz*, 1992a,b; *Bender et al.*, 1996]. In the south, the $O_2/N_2$ cycle is caused primarily by $O_2$ exchange with the oceans, while in the north the exchange of $O_2$ with the oceans and land biota both contribute significantly to the seasonal cycle [*Keeling and Shertz*, 1992b; *Keeling et al.*, 1993]. The cycles in the two hemispheres are largely decoupled from each other because of the slow mixing of air across the equator. In both hemispheres, air-sea exchange of $N_2$ caused by temperature-induced solubility changes in surface waters also makes a small contribution to the cycles [*Keeling and Shertz*, 1992b; *Keeling et al.*, 1993; *Bender et al.*, 1996]. In previous work, the seasonal cycles in the $O_2/N_2$ ratio have been used to derive constraints on rates of biological new production in the ocean [*Keeling and Shertz*, 1992b; *Bender et al.*, 1996] and to test biological ocean models [*Six and Maier-Reimer*, 1996]. Here we emphasize their additional importance as a constraint on the kinetics of air-sea gas exchange.

The oceans contribute to the $O_2/N_2$ cycles through seasonal variations in marine photosynthesis, respiration, and vertical water transports and by seasonal variations in $O_2$ and $N_2$ solubility in seawater induced by variations in water temperature and salinity. The air-sea $O_2$ exchanges are tied to observable variations in $O_2$ partial pressure or, equivalently, the $O_2$ saturation anomaly in surface seawater. Recently, *Najjar and Keeling* [1997] have compiled a monthly global climatology of the $O_2$ saturation anomaly using the global data set for dissolved $O_2$ concentration,

[1]Scripps Institution of Oceanography, University of California, San Diego, La Jolla.
[2]Department of Meteorology, Pennsylvania State University, University Park.
[3]Climate and Global Dynamics Division, National Center for Atmospheric Research, Boulder, Colorado.
[4]Department of Geophysical Sciences, University of Chicago, Chicago, Illinois.
[5]Max-Planck-Institut für Meteorologie, Hamburg, Germany.



Paper number 97GB02339.
0886-6236/98/97GB-02339$12.00

salinity, and temperature, archived at the National Oceanographic Data Center. This climatology, based on observations from years extending from 1898 through 1991, complements the atmospheric $O_2/N_2$ observations by providing additional information on the global air-sea $O_2$ exchanges and complements studies of $O_2$ cycling at local hydrographic stations [*Emerson et al.*, 1991; *Spitzer and Jenkins*, 1989; *Emerson*, 1987; *Jenkins and Goldman*, 1985] by providing a global perspective on the seasonal cycles in dissolved $O_2$ in the oceans. A summary of the *Najjar and Keeling* [1997] climatology is shown in Figure 1.

In this paper we present a summary of the seasonal cycles in $O_2/N_2$ observed in flasks collected from nine stations

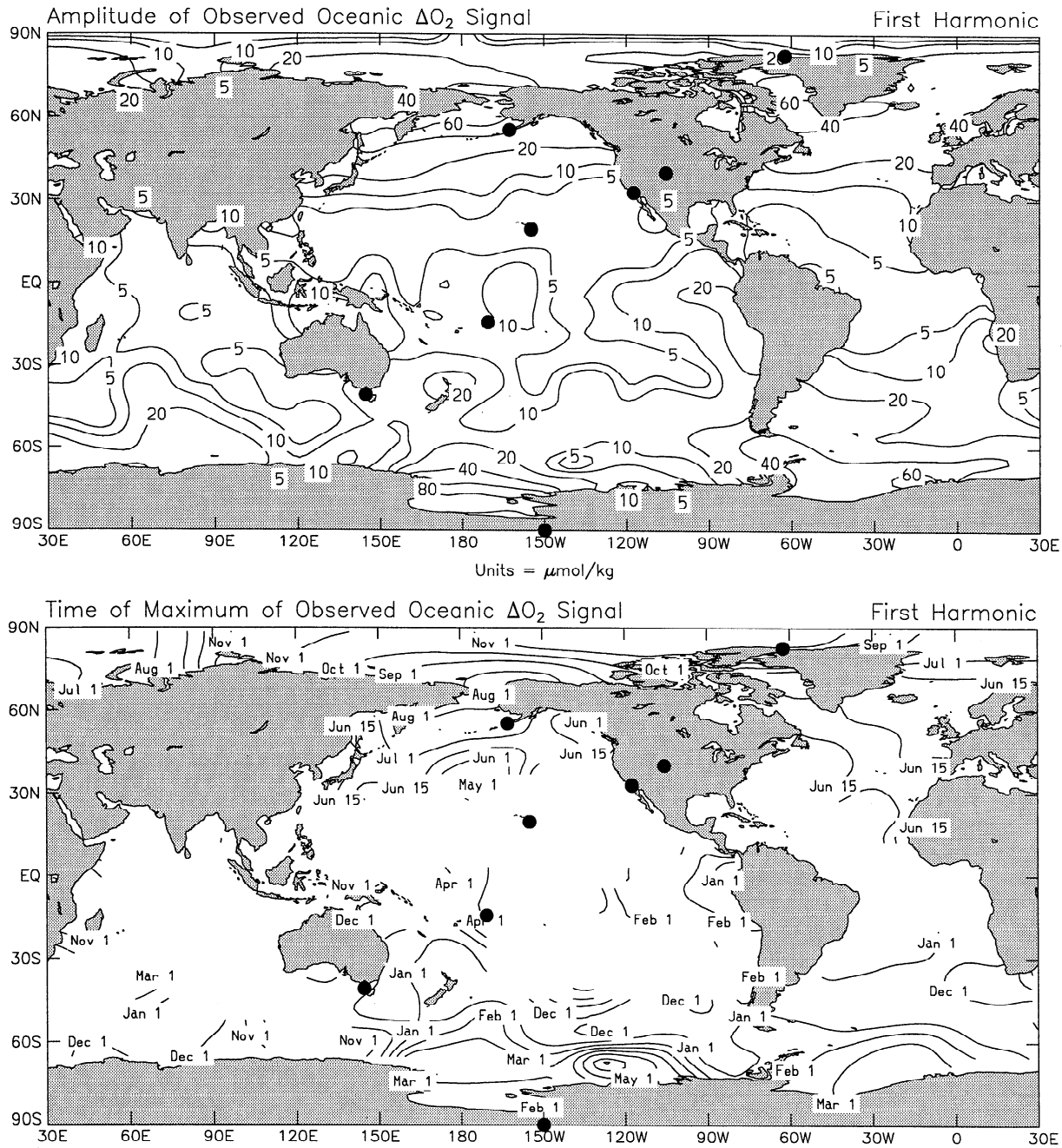


**Figure 1.** Peak-to-peak amplitude and phasing (time of maximum) of the first harmonic (fundamental) of the observed annual cycle in dissolved $O_2$ saturation anomaly in surface waters from the climatology of *Najjar and Keeling* [1997]. A temperature-based rescaling has been applied to the $O_2$ data (as detailed in Appendix A), and the data have been regridded onto an 8° × 10° (latitude times longitude) grid prior to contouring. The phase has been countoured only where the amplitude is greater than ±5 μmole $kg^{-1}$. Sampling stations (Table 1) for atmospheric $O_2/N_2$ measurements are indicated with solid circles, with Mauna Loa and Kumukahi indicated by a single circle.

sampled between 1989 and 1996. These results expand on the more limited data sets published in earlier studies [*Keeling and Shertz*, 1992a,b; *Bender et al.*, 1996; *Keeling et al.*, 1996]. Here we also develop a diagnostic model of these cycles that is partly based on the oceanic $O_2$ anomaly maps. The modeling exercise has two applications: (1) it provides a constraint on the magnitude of the air-sea gas-exchange velocity of $O_2$, and (2) it provides monthly maps of the air-sea $O_2$ flux that are "calibrated" against the atmospheric observations. In this paper we focus mainly on the constraint on gas-exchange velocities; the $O_2$ flux maps and their relationship to marine biogeochemical cycling of $O_2$ will be discussed elsewhere.

Briefly, the modeling approach is as follows: The $O_2$ anomaly maps are multiplied by maps of the air-sea gas-exchange velocity thus yielding maps of the monthly air-sea $O_2$ flux. Maps are also computed of the monthly air-sea $N_2$ flux based on the net air-sea heat flux. These $O_2$ and $N_2$ flux maps are then used to simulate seasonal variations in the $O_2/N_2$ ratio in an atmospheric tracer transport model. The simulated $O_2/N_2$ cycles are compared to the observed cycles after correcting the latter for the effects of terrestrial exchanges. By adjusting the magnitude of the gas-exchange velocity for $O_2$ to obtain an optimum fit between the simulated and observed cycles, we derive an independent estimate of the exchange velocity. The approach effectively invokes the mass balance of $O_2$ in the atmosphere on seasonal timescales. Because relatively little air is exchanged between the middle latitudes of the northern and southern hemispheres on a seasonal timescale, the method can provide independent constraints on the mean gas-exchange velocity in each hemisphere. This method is only one of three methods for constraining gas-exchange velocities on the large scale, the other two being based on the oceanic budgets of natural and bomb-produced radiocarbon [*Broecker and Peng*, 1974; *Broecker et al.*, 1985,1986]. Such constraints are important as they suggest the appropriate transfer velocities for computing large-scale fluxes, such as the uptake of anthropogenic $CO_2$ by the oceans [e.g., *Tans et al.*, 1990].

The exchange velocities derived from the $O_2$ mass balance can address an important outstanding question regarding the magnitude of gas exchange in the open ocean. The radiocarbon mass balance approach yields an average gas-exchange velocity of $CO_2$ that is about a factor of 2 larger than the exchange velocity expected from the extrapolation of small-scale observations on wind/wave facilities and lakes [*Liss and Merlivat*, 1986; *Wanninkhof*, 1992]. It is possible that the discrepancy may arise from anomalous enhancement of $CO_2$ exchange due to hydration reactions [*Berger and Libbey*, 1969], but the evidence for significant enhancement at typical wind speeds in the open ocean is lacking [*Emerson*, 1995; *Wanninkhof*, 1992]. Alternatively, the small-scale experiments may not account fully for all of the processes governing gas exchange in the open ocean [*Wanninkhof*, 1992]. The $O_2$ mass balance method can help to decide between these two possibilities by providing an independent estimate of the large-scale average gas-exchange velocity for a gas other than $CO_2$.

The $O_2$ mass balance method is subject to uncertainty resulting from the sparseness of the oceanic $O_2$ data, from uncertainty in the modeled atmospheric transport, and from bubble and covariance effects which complicate the relation between the monthly mean $O_2$ anomaly and the monthly mean flux. The method also depends on the presently untestable assumption that the interannual and interdecadal variations in the $O_2/N_2$ cycles can be neglected. This assumption is needed because the oceanic and atmospheric observations were made in different time periods. As we will show below, we find that the $O_2$ mass balance method, nevertheless, yields a useful constraint on the exchange velocities for the oceans poleward of about 30° in both hemispheres. We further find that the derived exchange velocities are largely consistent with the global mean velocity derived from the radiocarbon budgets, suggesting that the exchange of $O_2$ as well as $CO_2$ is enhanced in the open ocean by mechanisms that were not systematically accounted for in the small scale experiments upon which the *Liss and Merlivat* [1986] relation is based.

We first discuss the atmospheric observations, focussing on the seasonal component caused by air-sea gas exchange. We then describe an approach to modeling these cycles using the observed $O_2$ anomaly maps as the basis for computing the air-sea $O_2$ flux, and we discuss the optimization of this model in relation to the constraint on the average air-sea $O_2$ gas-exchange velocity. Finally, we discuss the significance of these results in relation to other constraints on air-sea gas exchange.

## 2. Atmospheric Observations

We present results from air samples collected at nine stations worldwide as summarized in Table 1 and Figure 1. Seven of these stations are effectively located in the marine boundary layer, and the remaining three are located at elevations of 2800 to 3800 m. All stations were selected to allow sampling under conditions that minimize the influences of local land biota and fossil-fuel burning. Appropriate sampling conditions are determined on the basis of local wind direction, wind speed, and, where available, additional chemical tracer concentrations. Samples are cryogenically dried to remove water vapor on collection and are analyzed at the Scripps Institution of Oceanography for $O_2/N_2$ ratios using an interferometric method [*Keeling and Shertz*, 1992b; *Keeling*, 1988] and analyzed for $CO_2$ concentration using a nondispersive infrared analyzer.

We combine the concurrently observed $O_2/N_2$ ratios and $CO_2$ concentrations to derive the quantity

$$\delta(O_2/N_2)_{oc} = \delta(O_2/N_2) + \frac{R_{O_2:C}}{0.2095} X_{CO_2} \quad (1)$$

**Table 1.** Sampling Stations in the Scripps $O_2/N_2$ Network

| Station Code | Site | Latitude | Longitude | Elevation in meters | Time Period |
|---|---|---|---|---|---|
| ALT | Alert, Northwest Territories | 82°27'N | 62°31'W | 210 | April 1991 to May 1996 |
| CBA | Cold Bay, Alaska | 55°12'N | 162°43'W | 25 | Aug. 1995 to Jul. 1996 |
| NWR | Niwot Ridge, Colorado | 40°03'N | 105°38'W | 3749 | April 1991 to Jan. 1993 |
| LJO | La Jolla, California | 32°52'N | 117°15' W | 20 | May 1989 to June 1996 |
| MLO | Mauna Loa, Hawaii | 19°32'N | 155°35'W | 3397 | Aug. 1993 to July 1996 |
| KUM | Kumukahi, Hawaii | 19°31'N | 154°49'W | 40 | June 1993 to July 1996 |
| SMO | Cape Matatula, American Samoa | 14°15'S | 170°34'W | 42 | June 1993 to July 1996 |
| CGO | Cape Grim, Tasmania | 40°41'S | 144°41'E | 94 | Jan. 1991 to July 1996 |
| SPO | South Pole Station | 89°59'S | 24°48'W | 2810 | Nov. 1991 to Feb. 1996 |

where $R_{O_2:C}$ represents the $O_2$:C exchange ratio for land photo-synthesis and respiration, where $\delta(O_2/N_2)$ is the deviation in the $O_2/N_2$ ratio from a reference multiplied by $10^6$ (here referred to as "per meg" units) defined according to

$$\delta(O_2/N_2) = \left( \frac{(O_2/N_2)_{sample}}{(O_2/N_2)_{reference}} - 1 \right) 10^6 \qquad (2)$$

and where $X_{CO_2}$ is the $CO_2$ mole fraction expressed as micromoles of $CO_2$ per mole of dry air. We assume $R_{O_2:C}$ = 1.1, based on evaluations of *Severinghaus* [1995]. The factor of 0.2095 is the $O_2$ mole fraction in dry air which is needed because $\delta(O_2/N_2)$ effectively measures $O_2$ changes relative to the total number of $O_2$ molecules, whereas $X_{CO_2}$ measures $CO_2$ changes relative to total dry air. The quantity $\delta(O_2/N_2)_{oc}$ is invariant to land biotic exchanges which produce compensating changes in $O_2$ and $CO_2$. The burning of liquid and gaseous fossil fuels, which have $O_2$:C combustion ratios higher than 1.1, causes $\delta(O_2/N_2)_{oc}$ to decrease. Exchanges of $O_2$, $CO_2$, or $N_2$ with the oceans will also cause $\delta(O_2/N_2)_{oc}$ to vary. Over the seasonal time frame, however, the contributions due to fossil-fuel burning [*Heimann and Keeling*, 1989] and oceanic exchanges of $CO_2$ [*Kurz*, 1993; *Erickson et al.*, 1996] are much smaller than the contributions due to exchanges of $O_2$ and $N_2$ with the oceans. To a good approximation, we are thus justified in interpreting the seasonal cycles in $\delta(O_2/N_2)_{oc}$ in terms of air-sea exchange of $O_2$ and $N_2$ alone.

To extract the seasonal component of the variations in $\delta(O_2/N_2)_{oc}$, we fit the time series in $\delta(O_2/N_2)_{oc}$ for each station to the sum of a slowly varying interannual function and a periodic annual function. At all stations except Cold Bay and Niwot Ridge, we used an interannual function consisting of a stiff spline fit and used a periodic function consisting of the first four harmonics of the annual cycle. For Cold Bay and Niwot Ridge, where the records are of short duration, we detrended the data by subtracting a fixed linear trend equal to the long-term average trend observed at La Jolla and fit the residuals to a periodic function consisting of the sum of the first two harmonics of the annual cycle. We found that the derived harmonic coefficients were relatively insensitive to the choice of the magnitude of the linear trend.

Results for the first two harmonic coefficients, expressed as the peak-to-peak amplitude and phase, are given in Table 2. Also given are 1-$\sigma$ error estimates based on the residuals from the least squares fit and the error contributions from uncertainty in the exchange coefficient with land biota, based on $R_{O_2:C}$ = 1.1±0.05. In the northern hemisphere, where the cycles in atmospheric $CO_2$ concentration are comparable in magnitude (on a mole-for-mole basis) to the

**Table 2.** Peak-to-Peak Amplitudes and Phasing of Harmonics of the Oceanic Component of the Seasonal Cycle in $\delta(O_2/N_2)$ at Background Stations[a].

| Station Code | First Harmonic (annual) | | | | | | Second Harmonic (semiannual) | | | | | |
|---|---|---|---|---|---|---|---|---|---|---|---|---|
| | Amp | $\sigma_{fit}$ | $\sigma_R$ | $T_{max}$ | $\sigma_{Fit}$ | $\sigma_R$ | Amp | $\sigma_{fit}$ | $\sigma_R$ | $T_{max}$ | $\sigma_{Fit}$ | $\sigma_R$ |
| ALT | 45.9 | 1.2 | 3.3 | 259.3 | 1.6 | 0.4 | 10.6 | 1.3 | 0.2 | 11.0 | 3.3 | 3.7 |
| CBA | 67.8 | 6.6 | 2.8 | 220.2 | 6.8 | 1.3 | 7.6 | 7.6 | 1.8 | 160.9 | 26.5 | 4.1 |
| NWR | 25.3 | 4.6 | 1.8 | 271.9 | 12.7 | 1.2 | 6.3 | 5.1 | 0.4 | 97.2 | 23.2 | 2.4 |
| LJO | 53.3 | 1.6 | 1.8 | 230.0 | 1.7 | 0.8 | 7.6 | 1.6 | 0.8 | 36.4 | 6.0 | 2.0 |
| MLO | 13.2 | 1.5 | 1.0 | 247.6 | 6.4 | 4.5 | 2.1 | 1.4 | 0.4 | 182.4 | 20.4 | 3.8 |
| KUM | 26.4 | 2.5 | 1.5 | 246.7 | 5.7 | 1.8 | 2.1 | 2.5 | 0.3 | 34.2 | 35.3 | 6.7 |
| SMO | 24.3 | 1.8 | 0.1 | 92.4 | 4.5 | 0.4 | 1.4 | 1.9 | 0.0 | 160.6 | 36.1 | 2.9 |
| CGO | 64.1 | 1.6 | 0.2 | 67.7 | 1.5 | 0.1 | 15.7 | 1.6 | 0.0 | 23.6 | 3.1 | 0.0 |
| SPO | 61.2 | 2.5 | 0.2 | 77.2 | 2.2 | 0.1 | 10.8 | 2.4 | 0.0 | 43.1 | 6.5 | 0.1 |

[a]Amplitudes (Amp) and corresponding uncertainties are expressed in per meg units; phasing ($T_{max}$) and corresponding uncertainties are expressed as the Julian dates of the maximum. Estimates are separately given of the 1-$\sigma$ error contributions from the residuals from the least squares fit ($\sigma_{fit}$) and from uncertainty in the exchange coefficient with land biota ($\sigma_R$). For the latter, we have allowed for error propagation assuming an exchange coefficient of $R_{O_2:C} = 1.10 \pm 0.05$.

cycles in $\delta(O_2/N_2)_{oc}$, the amplitudes of the cycles are sensitive to the value chosen for $R_{O_2:C}$, with a 10% variation in $R_{O_2:C}$ producing 3 to 7% changes in the $\delta(O_2/N_2)_{oc}$ amplitude, depending on the station. In the southern hemisphere, where the $CO_2$ cycles are much smaller, the sensitivity to $R_{O_2:C}$ is negligible.

The coefficients are also subject to uncertainty resulting from the interaction between fitting the periodic and interannual components of the trends. On the basis of the sensitivity of the harmonic coefficients to the selected spline stiffness, we believe these errors are negligible at the middle- and high-latitude stations, where the amplitudes of the cycles are large. These errors may be more significant, however, at the low-latitude stations of Kumukahi, Mauna Loa, and Samoa, where the amplitudes of the cycles are smaller. Such errors are hard to assess, and this complicates the interpretation of the tropical cycles. Longer records are needed to reduce such errors.

The interannually detrended observations based on $R_{O_2:C} = 1.1$ are plotted for each station in Figure 2. Observations from all years are plotted as though they were taken in a single "climatological" year. Statistically significant cycles are detected at all stations. The scatter of the data about the curve results from a combination of measurement errors, sampling errors, and short-term and interannual variability in $O_2/N_2$ and $CO_2$. Here we focus only on the quasi-regular cycles, represented by the smoothed curves.

A comparison of results at different stations (Figure 3) reveals several generally consistent patterns with latitude. The cycles in the northern hemisphere are roughly 6 months out of phase with the cycles in the southern hemisphere, with the cycles at the extreme northern and southern sites almost perfectly diametrically out of phase. The stations with the largest amplitudes and earliest phasing are found at middle latitudes, with Cape Grim and Cold Bay having the largest amplitude and earliest phasing in the southern and northern hemispheres, respectively. The cycles at the middle and high latitudes of the southern and northern hemisphere are similar in amplitude, though the cycles in the south appear to have sharper maxima than the cycles in the north. In both hemispheres, the maxima tend to occur near the middle of the summer, while the minima occur in the late winter or early spring. This timing of the atmospheric cycles largely reflects the timing of seasonal ingassing and outgassing resulting from both biological and thermal forcing in the oceans [*Keeling and Shertz*, 1992a; *Bender et al.*, 1996; *Najjar and Keeling*, 1997].

Some differences can be noted in the shape of the cycles at the Northern Hemisphere stations. At Alert, and possibly also at Cold Bay, the maximum is of longer duration than the minimum, while at La Jolla, and possibly also at Niwot Ridge, the opposite is true. Niwot Ridge is an exceptional midlatitude station, being located well above sea level and remote from the ocean. The amplitude here is much smaller, and the phasing lagged relative to the cycles seen at stations immediately to the north and south, as may be expected from the greater horizontal and vertical distance from the ocean.

Smaller amplitudes are detected at the tropical stations of Mauna Loa, Kumukahi, and Samoa. The curve fits to the Kumukahi and Mauna Loa stations show double maxima, although this feature is weak and probably not statistically significant. The phasing at Mauna Loa and Kumukahi is

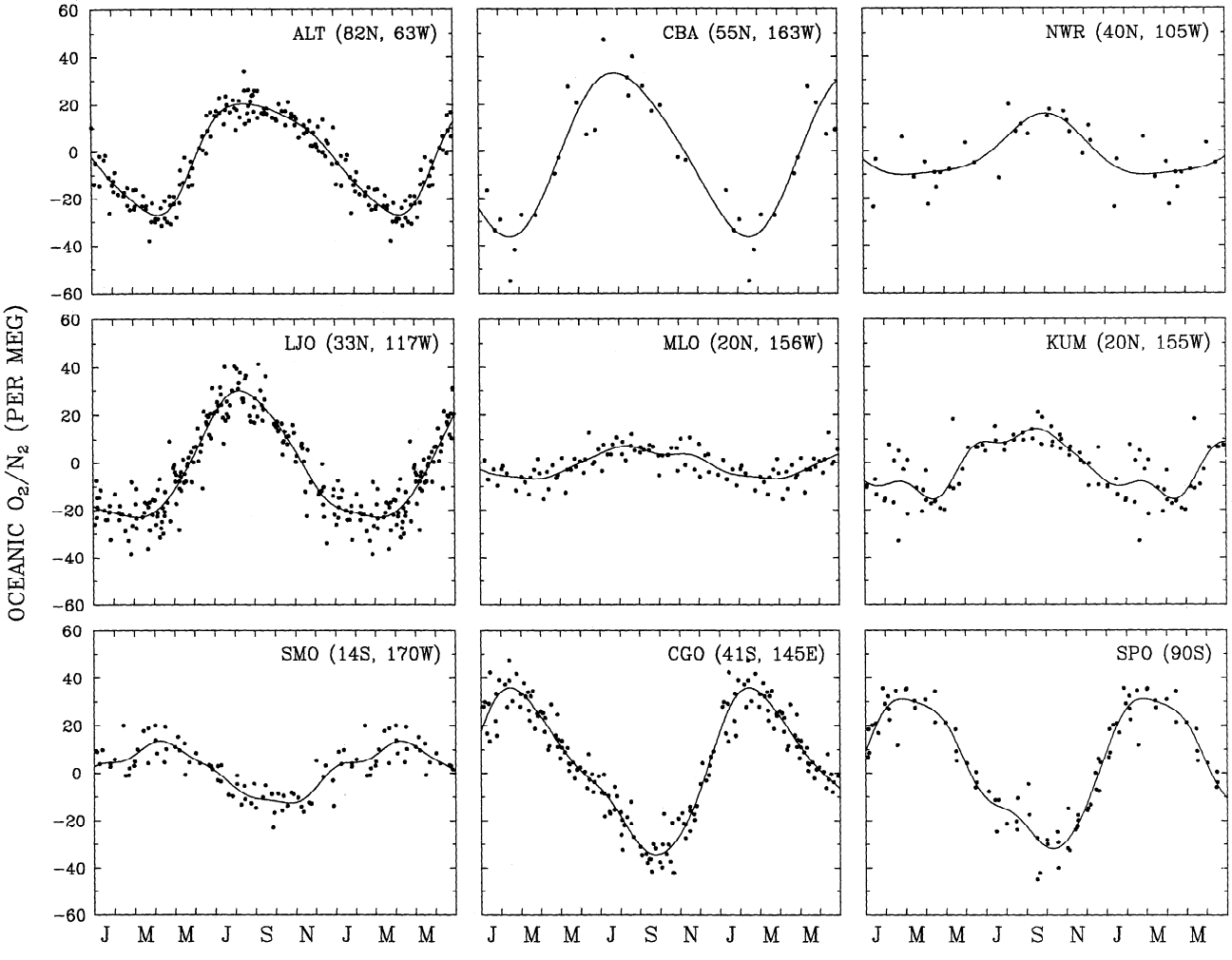


**Figure 2.** Circles represent observed oceanic component of the seasonal cycle in the atmospheric $O_2/N_2$ ratio computed according to equation (1). Individual data points reflect the average of the analyses of two or three replicate flasks collected simultaneously. The ratios have been corrected for terrestrial exchanges using concurrent $CO_2$ data (using an $O_2$:C ratio of 1.1) and have been interannually detrended. Observations for several years are plotted against a single climatological year. The curve is a least-squares fit to the seasonal cycles based on a periodic function containing two to four harmonics (Table 2). Except at CBA and NWR, the curves include the fundamental plus three additional harmonics of the annual cycle. At CBA and NWR, only the fundamental annual and semiannual harmonics are used owing to the limited seasonal coverage.

similar to the stations farther to the north, and the phasing at Samoa is similar to stations to the south. This is in accord with the general understanding that air exchange within each hemisphere is more rapid than the exchange across the equator.

The amplitude at Mauna Loa is only 50% of that at Kumukahi when expressed in terms of the statistically significant fundamental harmonic component (Table 2). The Kumukahi and Mauna Loa stations are located only 83 km horizontally from each other, so the difference must be the result of vertical gradients in concentration. It is possible that these gradients are maintained by the trade wind inversion, which typically lies at an elevation between the two stations and which separates air mixed convectively in the marine boundary layer from subsiding air in the free troposphere associated with the sinking branch of the Hadley circulation. The phasing of the fundamental harmonic component at Mauna Loa is synchronous with the phasing at Kumukahi to within the uncertainties.

A minimum in the seasonal amplitude is inevitable at some zone in the tropics because of mixing of signals counterpropagating from either hemisphere that may destructively interfere. The interference mechanism may also lead to a change in the phasing of the seasonal cycle depending on the relative fraction of air from the two hemispheres as well as the time lag for air parcels to cross the equator. For example, a component from the other hemisphere, having originated 180° out of phase and having

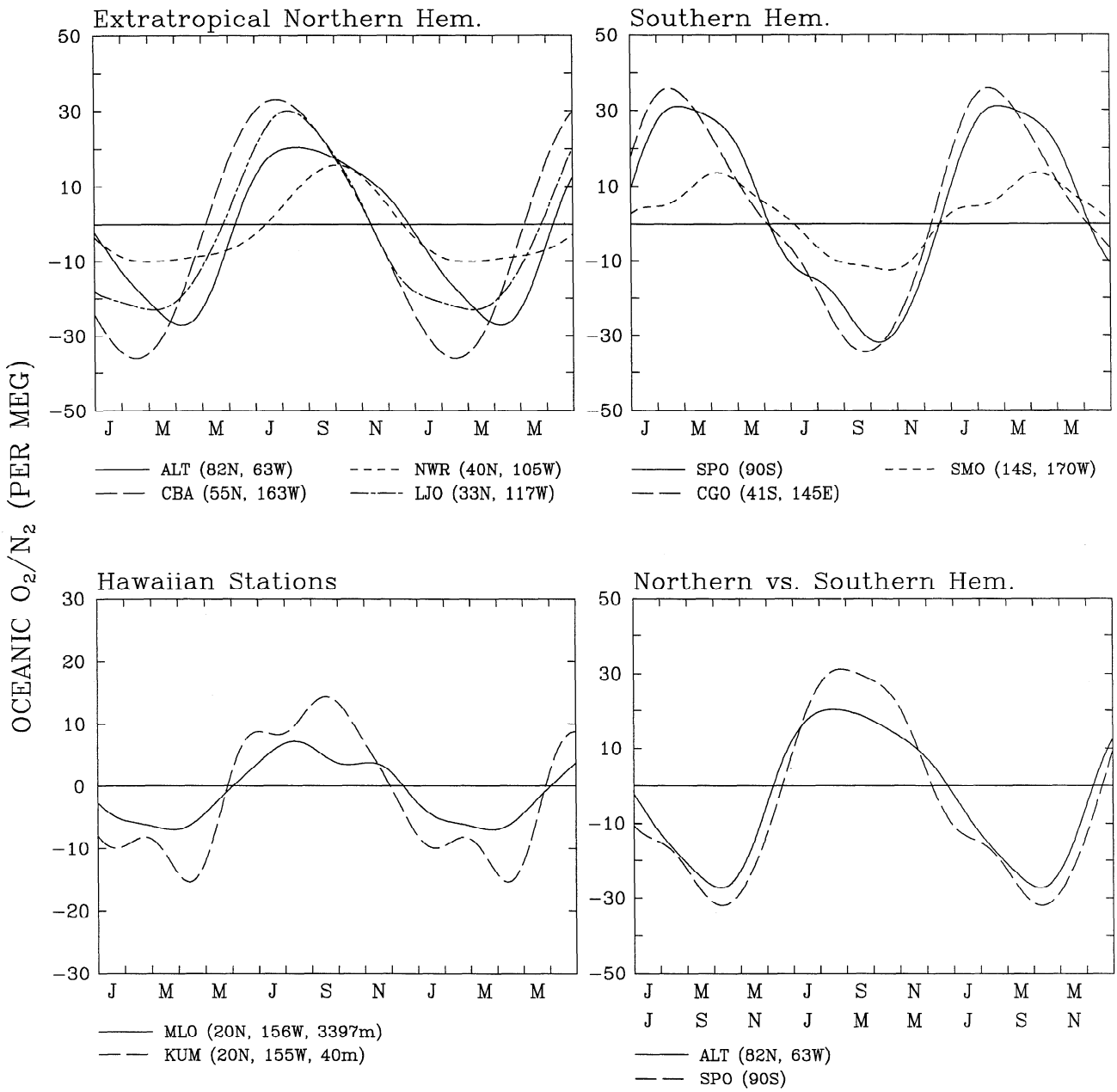


**Figure 3.** Comparison of fitted curves to the observed oceanic components of the seasonal $O_2/N_2$ cycles at different stations. Note the different scale for the Hawaiian stations, and note that the phasing for the south pole has been reversed in the last graph to assist in the comparison with the cycle at Alert.

suffered an additional phase lag, would effectively have advanced phasing relative to the component from within the hemisphere. One possible explanation of the small amplitude at Mauna Loa is that it arises from such an interference mechanism. If the southern component at Mauna Loa were transported with the descending branch of the Hadley circulation, then the trade wind inversion would block this component from influencing the cycle at Kumukahi. If this mechanism is correct, it requires that a significant fraction of the air entering the ascending branch of the Hadley cell and advected to the latitude and elevation of Mauna Loa is of recent southern-hemispheric origin.

## 3. Air-Sea $O_2$ Flux Computation

We now attempt to simulate the observed $O_2/N_2$ cycles based on a model driven by oceanic $O_2$ and $N_2$ fluxes. Air-sea $O_2$ fluxes can be computed according to

$$F_{O_2} = K_{O_2}\left(\Delta[O_2] - \Delta[O_2]_{bub}\right) \quad (3)$$

where $K_{O_2}$ is the gas-exchange velocity for $O_2$, $\Delta[O_2]$ is the $O_2$ anomaly, and $\Delta[O_2]_{bub}$ is the steady state $O_2$ anomaly required to balance $O_2$ injected below the surface by

bubbles [*Keeling*, 1993]. Neglecting $\Delta[O_2]_{bub}$ and averaging (3) over a monthly time scale, we obtain

$$\overline{F_{O_2}} = \overline{K_{O_2}} \cdot \overline{\Delta[O_2]} + \overline{K'_{O_2} \cdot \Delta[O_2]'} \quad (4)$$

where the overbar ($^-$) and prime ($'$) denote the monthly average and deviation from the monthly average, respectively. The first term in (4) reflects the flux contribution due to the product of the monthly mean anomaly and the monthly mean gas-exchange velocity, and the second term reflects short-term covariance of anomaly and exchange velocity. In the simulations here, we account only for the first term on the right-hand side of (4). The bubble term in (3) and the covariance term in (4) are addressed in Appendices B and C. While these terms may be important for computing annual-averaged fluxes or other quantities, we find that their contributions to the seasonal variations in the fluxes appear to be relatively small.

To evaluate $\overline{\Delta[O_2]}$ in (4), we use the $O_2$ anomaly maps of *Najjar and Keeling* [1997] after correcting the maps for variations in sea level pressure as described by *Najjar and Keeling* [1997] and correcting for the skin temperature effect using the formula of *Hasse* [1971], with a depth for the bulk temperature measurement of 2.5 m and with heat fluxes from the atlas of *Oberhuber* [1988] and wind speeds from *Wright* [1988]. These $O_2$ anomaly maps may underestimate the seasonal amplitudes in regions of sparse data, where the maps are based on 3-month or 5-month running averages. *Najjar and Keeling* [1997] found that sea surface temperature maps prepared with the same computational methods and data resolution as the $O_2$ anomaly maps yield smaller seasonal amplitudes as compared to the temperature maps of *Shea et al.* [1992], which are based on a much more extensive data set. These temperature amplitudes are about 10% lower in the northern hemisphere and range up to 50% lower in certain zones of the southern hemisphere compared to the amplitudes computed from the higher density data set. We expect that the seasonal amplitudes in the $O_2$ anomaly may be underestimated by similar factors, and we therefore use the temperature data to adjust the $O_2$ anomaly maps as described in Appendix A. This procedure represents our best attempt at preparing maps with the correct seasonal amplitudes, although we recognize that it cannot fully compensate for the deficiencies arising from data sparseness because the seasonal cycles in the $O_2$ anomaly and temperature do not necessarily have similar shapes in the ocean. We expect that uncertainties in the corrected maps are comparable in magnitude to the corrections themselves.

To evaluate the monthly mean gas-exchange velocity $\overline{K_{O_2}}$ in (4), we use alternatively three formulations for the transfer velocity: (1) the *Wanninkhof* [1992] formula appropriate for time-averaged winds, (2) the *Liss and Merlivat* [1986] formula, and (3) a constant transfer velocity in space and time. The Wanninkhof formula assumes $K_i = 0.39\, u_{av}^2 (Sc_i/660)^{-1/2}$, where $K_i$ (cm/hr) and $Sc_i = \nu/D_i$ are the exchange velocity and the temperature-dependent Schmidt number of constituent $i$, respectively ($\nu$ is the kinematic viscosity of seawater and $D_i$ is the molecular diffusivity of the gas in seawater), $u_{av}$ (m/s) is the long-term average wind speed, and 0.39 is a constant adjusted to match the large-scale mass balance constraints for radiocarbon. For $u_{av}$, we use monthly averaged 10-m surface wind speeds from a climatology over the years 1981-1993 computed from the reanalyses of the European Centre for Medium-Range Weather Forecasts (ECMWF) model [*Gibson et al.*, 1997]. For the Schmidt number, we use the relation $Sc_{O_2} = 1638 - 81.83T + 1.483T^2 - 0.008004T^3$ (temperature ($T$) is in degrees Celsius) with the monthly mean sea surface temperatures from *Shea et al.* [1992]. We derived this Schimdt number/temperature relation based on the compilation of freshwater measurements by *Jähne* [1980], as reported by *Liss and Merlivat* [1986], after correcting the values upward by a factor of 1.13 for the expected difference between freshwater and salt water [*Wanninkhof*, 1992]. In regions of sea ice specified by *Shea et al.* [1992], we set the transfer velocity to zero. We use the same wind speed and temperature data for the simulations using the Liss and Merlivat formulation. For the third formulation, the exchange velocity is fixed at 22.5 cm/hr in ice-free regions and set to zero in ice-covered regions. The value of 22.5 cm/hr is the average of the gas-exchange velocity computed from the Wanninkhof relation with the ECMWF winds in ice-free regions.

## 4. Air-Sea $N_2$ Flux Computation

We compute monthly maps of the thermally driven flux of $N_2$ between the air and sea following the procedure of *Keeling et al.* [1993] in which the gas flux is assumed to be proportional to the net air-sea heat flux multiplied by the temperature derivative of the $N_2$ solubility. The calculation effectively assumes that gas exchange is sufficiently rapid to maintain dissolved $N_2$ in equilibrium with atmospheric $N_2$ during the course of seasonal temperature changes in the mixed layer. With this approach, the computed $N_2$ fluxes are independent of the magnitude of the gas-exchange velocity. In regions of sea ice, we set the $N_2$ flux equal to zero because heat transfer likely leads to changes in the amount of sea ice, rather than to changes in sea surface temperature which would lead to changes in $N_2$ solubility. For these computations, we have used monthly net heat fluxes from the ECMWF climatology [*Gibson et al.*, 1997] combined with $N_2$ solubilities from *Weiss* [1970].

## 5. Atmospheric Simulations

We impose the monthly maps of $O_2$ and $N_2$ flux as a lower boundary condition to the TM2 atmospheric tracer transport model [Heimann, 1995], which calculates the

three-dimensional advection from 12-hourly wind fields from the ECMWF meteorological analyses for 1987. We take results from the fourth year after initialization, when the simulated seasonal cycles have stabilized. Because the transport model is linear in tracer concentration, we can simulate various components of the source fields separately and sum the results for comparison with the atmospheric data. A list of the components that we have run separately is given in Table 3. For the purpose of comparing with the "climatological" observations, we use only a low-passed filtered representation of the model output consisting of the sum of the fundamental and three additional harmonics of annual cycles.

Figure 4 shows results of simulations at the baseline stations for three components: (1) the $N_2$ component, (2) the $O_2$ component calculated from the temperature-scaled $O_2$ anomaly maps and the Wanninkhof gas-exchange relation with ECMWF winds, and (3) the composite cycle derived by summing the $N_2$ and $O_2$ components. Also shown for comparison is the observed cycle in $\delta(O_2/N_2)_{oc}$, which, as we have noted, can be interpreted in terms of oceanic exchange of $O_2$ and $N_2$ alone. The modeled cycles are dominated by $O_2$ components, with the $N_2$ component being generally about 5 times smaller than and nearly out of phase with the observed $O_2/N_2$ cycles. The proportions correspond to an aggregate $O_2$:$N_2$ flux ratio of approximately 1.35, considering that air contains 3.7 times as much $N_2$ as $O_2$.

The model accounts for many general features of the observations. The simulated amplitudes agree within a factor of 2, and the timing of the simulated zero-crossing agrees within 6 weeks with the observations at all stations. The shape and amplitude of the cycles is reasonably well simulated at Alert, Cape Grim, and the south pole. The model accounts qualitatively for the relative amplitudes and phase shifts between Cape Grim and the south pole in the southern hemisphere and Cold Bay and Alert in the northern hemisphere, and it accounts for the sharper maxima in the southern hemisphere.

The model, however, has a number of deficiencies. The simulated amplitudes are too large at Samoa and too small at La Jolla, Cape Grim, and the south pole. The model amplitude of the fundamental harmonic component at Mauna Loa is 80% as large as that at Kumukahi, whereas the observations indicate an amplitude only 50% as large. The model also does not account well for the shape of the maxima and minima at a number of stations. At Kumukahi, the simulated cycles have a high-frequency component that induces pronounced double maxima occurring in July and November, while the observations, at best, support only a much weaker double maxima occurring in June and September. The simulated cycles at Mauna Loa show similar double maxima that are also larger than the (probably insignificant) double maxima shown in the curve fit to the observations. At Samoa, the simulated cycles show a sharp minimum in November that is not observed.

To aid in understanding the origin of $O_2$ cycles at the individual stations, we separate the $O_2$ sources/sinks at each grid point into a (stationary) annual mean component and a

**Table 3.** $O_2$ and $N_2$ Source Components Used in the Tracer Transport Model

| Component | $O_2$ Anomaly Map | $V_{exch}$[a] | Latitude Band | Locally Balanced | Seasonally Varying |
|---|---|---|---|---|---|
| *$O_2$ Components* | | | | | |
| 1 | unscaled | W | globe | no | yes |
| 2 | temperature scaled | W | globe | no | yes |
| 2a | temperature scaled, annually adjusted | W | 31.3° to 90°N | yes | yes |
| 2b | temperature scaled, annually adjusted | W | equator to 31.3°N | yes | yes |
| 2c | temperature scaled, annually adjusted | W | 31.3°S to equator | yes | yes |
| 2d | temperature scaled, annually adjusted | W | 90° to 31.3°S | yes | yes |
| 2e | temperature scaled, annually averaged | W | globe | no | no |
| 3 | temperature scaled | LM | globe | no | yes |
| 4 | temperature scaled | C | globe | no | yes |
| *$N_2$ Component* | | | | | |
| 5 | N/A[b] | N/A | globe | no | yes |

N/A, not applicable.

[a]W: *Wannkinkhof* [1992]; LM: *Liss and Merlivat* [1986]; C: constant, see text.

[b]$N_2$ fluxes derived from ECMWF-based net air-sea heat flux climatology (*Gibson et al.*, 1997), see text.

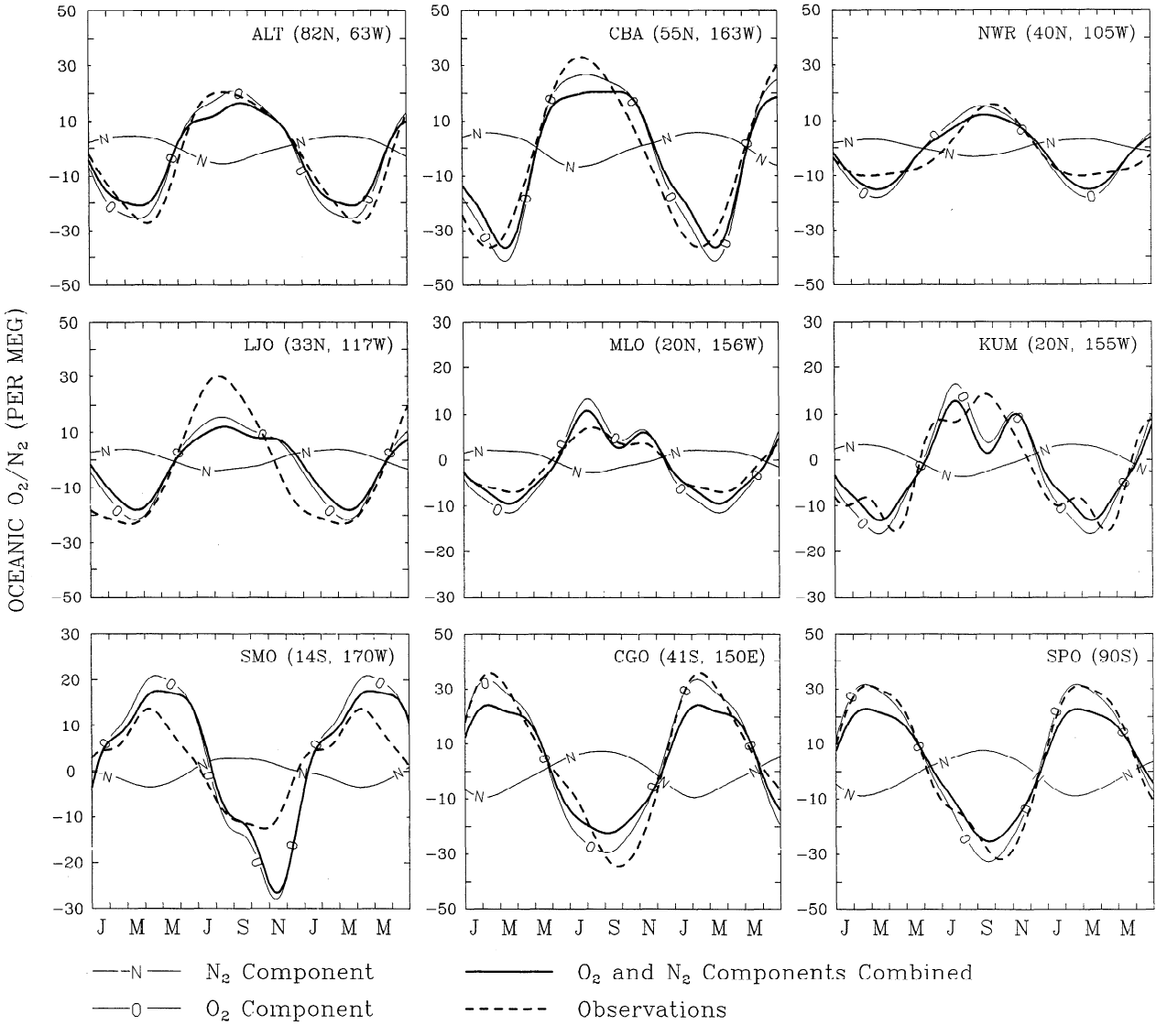


**Figure 4.** Simulated and observed oceanic components of the atmospheric $O_2/N_2$ cycle. The simulated $O_2$ component of the $O_2/N_2$ cycle is based on the temperature-scaled $O_2$ anomaly maps and on the Wanninkhof/ECMWF gas-exchange rates (component 2 in Table 3). The $N_2$ component is based on net heat flux data. The bold solid curve is the sum of these two components. Also shown for comparison is the observed oceanic $O_2/N_2$ cycle driven by air-sea exchanges of $O_2$ and $N_2$ using a terrestrial $O_2$:C ratio of 1.1. Note that the vertical scales are not all the same.

purely seasonal component with zero annual mean. We further subdivide the purely seasonal component into four zonal regions: 90°S to 31.3°S, 31.3°S to the equator, the equator to 31.3°N, and 31.3°N to the 90°N (see Table 3), and we run these components separately in the transport model. We chose a boundary near 30° in order to separate the influences of air-sea $O_2$ exchange from low latitudes, where the cycles in $\overline{\Delta[O_2]}$ are relatively small, from the influences of higher latitudes, where the cycles are larger; the precise latitude of 31.3° lies at a boundary between surface boxes in the TM2 model. The separate contributions to the model atmospheric cycles at the baseline stations are shown in Figure 5.

The annual-mean component can only contribute to seasonal variations through seasonal variations in atmospheric transport. We find that this component is negligible at all stations. The seasonal components from different zonal bands make unequal contributions to the cycles. At the middle- and high-latitude northern stations (Alert, Cold Bay, Niwot Ridge, and La Jolla), the cycle is dominated by seasonal air-sea exchange occurring north of 31°N. Similarly, at the middle- and high-latitude southern stations (Cape Grim and the south pole), the cycles are dominated by $O_2$ exchanges occurring south of 31°S. The cycles at the tropical stations (Mauna Loa, Kumukahi, and Samoa) are determined by a mixture of high-latitude and

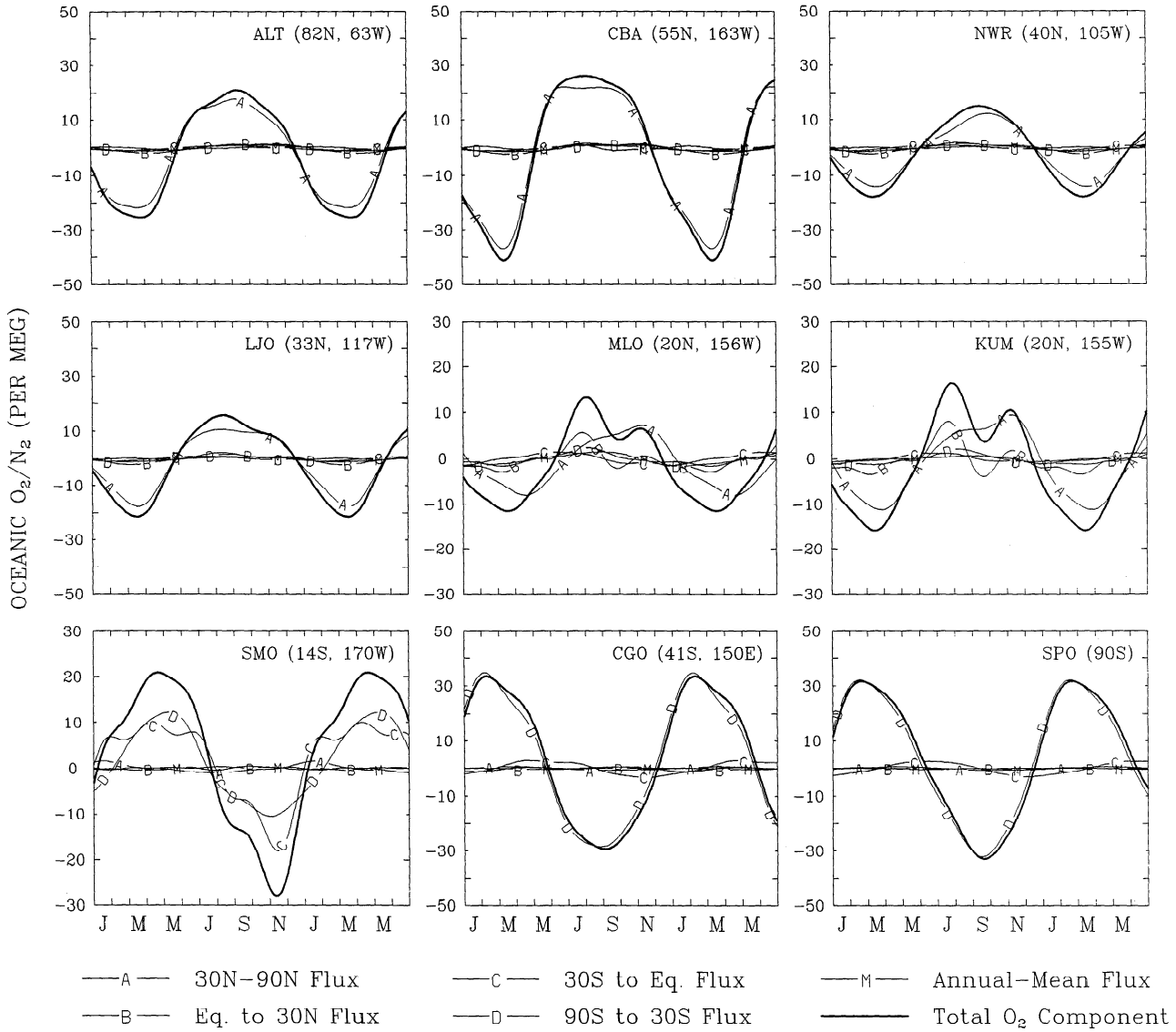


**Figure 5.** The contributions of flux components from different latitude zones and from annual-mean $O_2$ fluxes to the total $O_2$ component (curve labeled O in Figure 4). Note that vertical scales are not all the same.

low-latitude exchanges from within the hemisphere of the station. The high-latitude contribution consists of a relatively smooth sinusoidal function, while the low-latitude contribution shows more seasonal structure. The phasing of the high-latitude and low-latitude contributions is such that these components tend to reinforce each other in the tropics. Tropical exchanges are responsible for the simulated double maxima at Mauna Loa and Kumukahi and for the sharp November minimum at Samoa. The model does not yield a significant interference between northern and southern signals at Mauna Loa in contrast to our expectations based on observations discussed earlier.

The sensitivity of the simulations at high latitudes to the temperature-based scaling of the $O_2$ anomaly maps is shown in Figure 6. Using unscaled $O_2$ anomaly maps has little effect on the simulations in the northern hemisphere and in the tropics (not shown) but reduces the amplitudes at the southern hemisphere stations of Cape Grim and the south pole by about 30%. Adjusting the anomaly maps using our temperature-scaling technique considerably improves the simulations at these stations.

Simulations using different formulations for the gas-exchange velocity are shown in Figure 7. A constant gas-exchange velocity yields cycles with generally similar amplitudes to those simulated using the Wanninkhof/ECMWF exchange velocities. With constant velocity, the cycles have narrower maxima at Alert and Cold Bay, the cycle at Cold Bay being in somewhat better agreement with the observations. The Liss and Merlivat formulation yields cycles that are about a factor of 2 or more smaller. The simulated nitrogen component of the cycles, which offsets the $O_2$ component and is

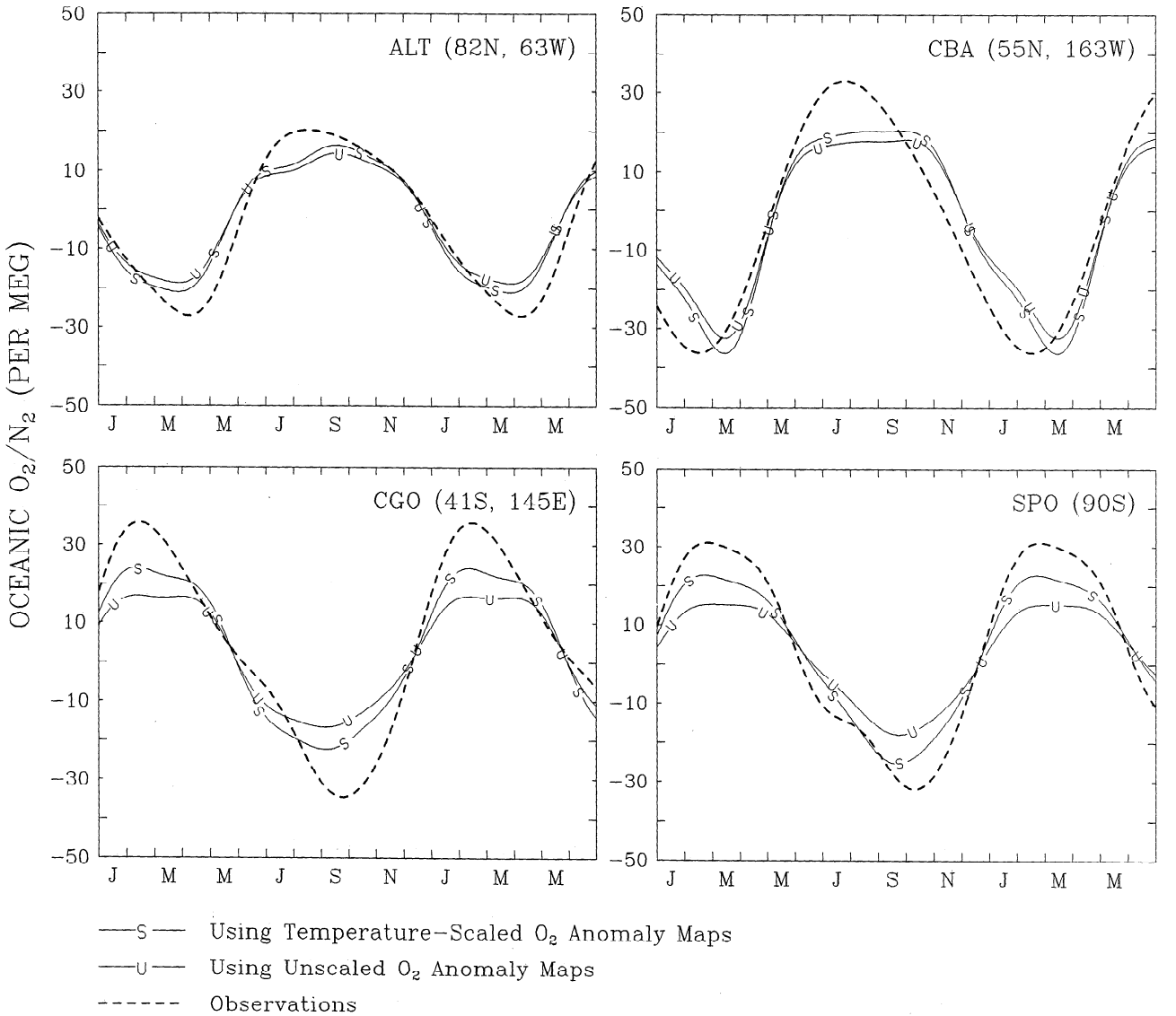


Figure 6. Comparison of the simulated oceanic component of the atmospheric $O_2/N_2$ cycles both with and without the temperature-based scaling of the $O_2$ anomaly fields. The curve labeled S represents the composite $O_2/N_2$ cycle using the scaled $O_2$ anomaly maps (same as the bold solid curve in Figure 4); the curve labeled U represents the composite $O_2/N_2$ cycle using the $O_2$ anomaly maps without temperature-based scaling. Both curves include the $N_2$ component. The dashed curve represents the observed cycle based on least squares fit to the observations using a terrestrial $O_2$:C ratio of 1.1. Note that vertical scales are not all the same.

computationally independent of the gas-exchange velocity, has a larger proportional influence on the simulations using the Liss and Merlivat/ECMWF exchange velocities because of the smaller $O_2$ component. Allowing for this $N_2$ component, the relative amplitudes predicted using different gas-exchange formulations are largely explained by the differences in the global average gas-exchange velocity for each formulation.

## 6. Model Optimization

We can achieve a better match between the predicted and observed cycles by optimally adjusting gas-exchange velocity for $O_2$. To this end, we fix the $N_2$ component but allow the $O_2$ component to be scaled arbitrarily by a multiplicative constant. We can interpret this constant as a correction factor for the gas-exchange velocity because the simulated atmospheric $O_2$ cycles are directly proportional to the gas-exchange velocity. We derive the optimum correction factor using an algorithm [*Heimann and Keeling*, 1989] that minimizes an error function equal to the sum of the squares of the differences between the observed and simulated harmonic components inversely weighted by the uncertainty in the observed harmonics. For these optimizations, we use the first two harmonics at Cold Bay and Niwot Ridge and the first four harmonics at the

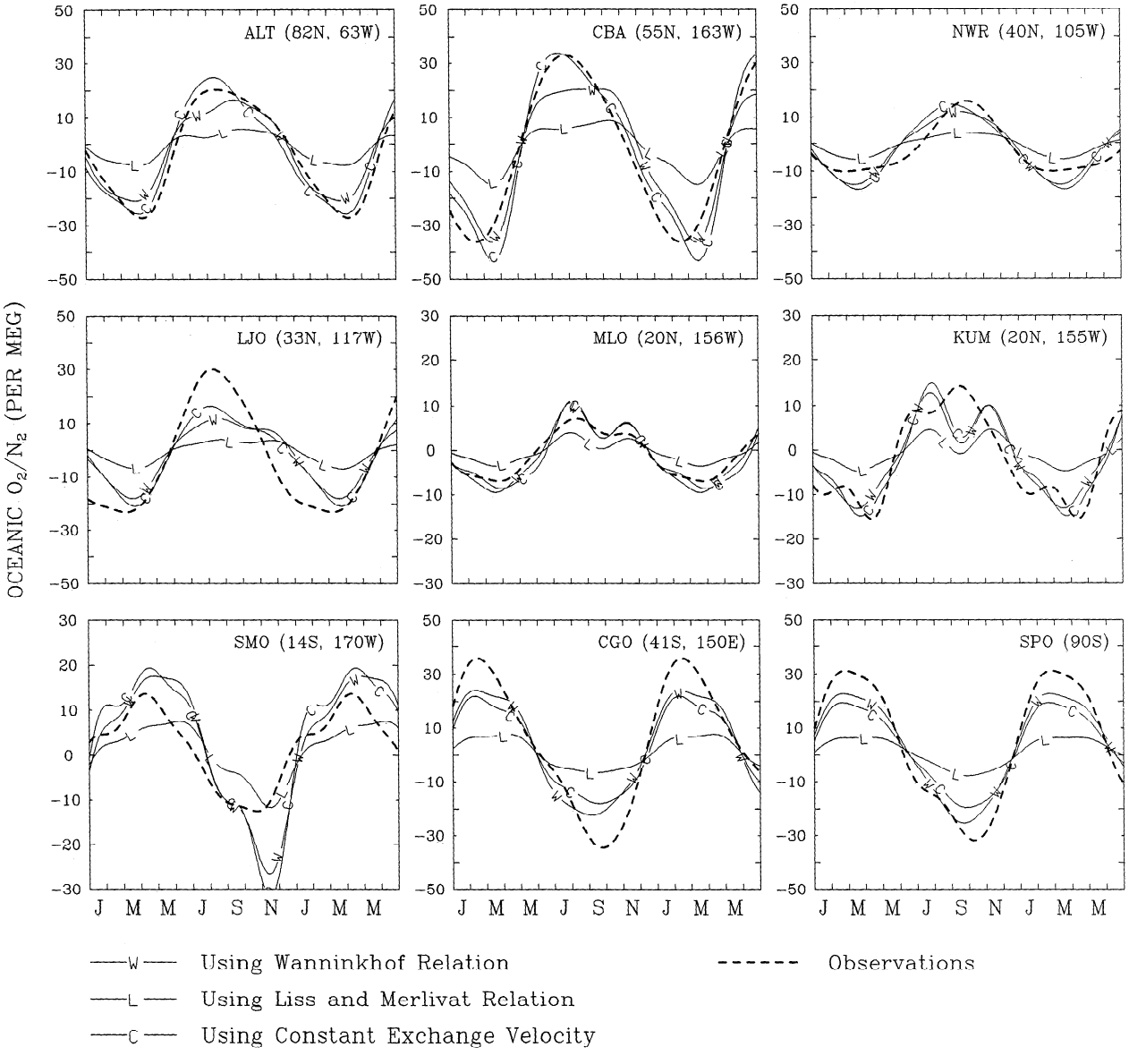


Figure 7. Comparison of the simulated oceanic component of the atmospheric $O_2/N_2$ cycles using different formulations of the air-sea gas-exchange velocity. The curve labeled W represents the composite cycle using the Wanninkhof/ECMWF gas-exchange velocities (same as the bold solid curve in Figure 4); the curve labeled L represents the composite cycle using the Liss and Merlivat/ECMWF gas-exchange coefficients; the curve labeled C represents the composite cycle using the constant gas-exchange velocity (see text). The dashed curve represents the observed cycle based on least squares fit to the observations using terrestrial $O_2$:C ratio of 1.1. Note that vertical scales are not all the same.

remaining stations. Generally, only the first one or two harmonics have significant statistical weight.

The optimum rescaling factors for simulations using the Wanninkhof/ECMWF gas-exchange velocities and using different stations, individually or in combination, are given in Table 4. Rescaling factors obtained for high-latitude stations in both hemispheres are between 1.0 and 1.24, indicating that the Wanninkhof/ECMWF exchange velocities are virtually optimal without adjustment. Rescaling factors well below 1.0 are required at Mauna Loa and Samoa. An unusually large rescaling factor of 1.59 is required at La Jolla. Obviously, with different factors needed at different stations, we cannot simultaneously optimize the simulations at all stations by a simple global rescaling of the gas-exchange velocity.

Recalling that the cycles at the middle- and high-latitude stations are mainly sensitive to gas exchange poleward of 31° in the respective hemisphere, we can construct an optimum rescaling factor for these regions in isolation. For the region north of 31°N, we use observations at Alert, Cold Bay, and Niwot Ridge, and for the region south of 31°S, we use observations from the Cape Grim and the

**Table 4.** Scale Factors for Optimal Fits

| Station(s) | Scale Factor |
|---|---|
| ALT | 1.16 ± 0.09 |
| CBA | 1.11 ± 0.12 |
| NWR | 0.94 ± 0.11 |
| LJO | 1.59 ± 0.25 |
| MLO | 0.81 ± 0.05 |
| KUM | 1.05 ± 0.19 |
| SMO | 0.61 ± 0.10 |
| CGO | 1.24 ± 0.10 |
| SPO | 1.22 ± 0.54 |
| ALT, NWR, CBA | 1.15 ± 0.05 |
| CGO, SPO | 1.23 ± 0.06 |
| All Stations | 1.14 ± 0.05 |

The uncertainties represent the standard errors to the fits based on the uncertainties in the observed harmonics (see Table 2.)

south pole. We thus derive optimal rescaling factors for gas exchange poleward of 31° of 1.15± 0.05 and 1.23±0.06 in the northern and southern hemispheres, respectively, where the uncertainties are the standard error to the fit based on the imprecision in the observed harmonic coefficients but do not include possible errors in model parameters.

In these optimizations, we have chosen to ignore results from La Jolla and the tropical stations. We have ignored results from La Jolla because of differences in the way the actual atmosphere and the model are sampled. To avoid local pollution during sampling at La Jolla, the samples are collected only during steady west-wind conditions. In the fall and winter, when the prevailing winds are off the land, these conditions generally occur only in association with episodic storm systems. In contrast, the model results are based on time averages regardless of wind direction. Thus we expect the observations may indicate a larger oceanic cycle than the model simply because the observations are biased toward conditions when the air is blowing off the ocean. In the future, we need to develop strategies for sampling the output of tracer transport models in a way that mimics the criteria used for collecting actual samples [*Erickson et al.*, 1996; *Ramonet and Monfray*, 1996]. Similar difficulties may effect the comparison at other stations, although these are probably less serious than at La Jolla.

We have chosen to ignore the results from the tropical stations because the model simulations indicate that the cycles at these stations are sensitive not only to exchanges poleward of 31° but also to low-latitude exchanges. Thus we cannot use these stations to uniquely constrain gas exchange in the poleward regions without first validating the low-latitude exchanges.

In principle, however, we can reverse the order of optimization and use the observations at the tropical stations to constrain gas exchange at low latitudes having first adjusted the gas exchange at higher latitudes to match the middle- and high-latitude stations. Fixing the gas exchange at higher latitudes using the above optimizations and uniformly rescaling the exchange velocity from 31°S to 31°N to match the observations at individual tropical stations stations requires a rescaling factor of 0.53±0.25 at Kumukahi, 0.48±0.49 at Mauna Loa, and 0.07±0.18 at Samoa, where the uncertainties are the standard errors to the fit based on the imprecision in the observed harmonic coefficients. Taken together, the optimizations appear to indicate that low-latitude gas exchange is substantially overpredicted by the Wanninkhof relation. The errors are large, however, and we do not feel that this interpretation, which results from the discrepancy between modeled and observed cycles in the tropics, can yet be taken seriously.

In the tropics, the $O_2$ anomaly maps are uncertain because of the small seasonal signals (Figure 1), poor data coverage, and potentially large interannual variations associated with El Niño/Southern Oscillation phenomena that may have been aliased in producing the $O_2$ anomaly maps [*Najjar and Keeling*, 1997]. Interannual variability also complicates the determination of the atmospheric cycles in the tropics, as discussed earlier. The tropical cycles are also sensitive to atmospheric transports over long distances, such as signals propagating from both high and low latitudes within the hemisphere and by signals transported across the equator. The failure of the model to reproduce the Mauna Loa/Kumukahi amplitude ratio may indicate that the model underestimates the importance of the interference between signals counterpropagating from the the north and south. Although the TM2 model has been shown to yield realistic simulations of north-south gradients in $^{85}Kr$ and F11 [*Heimann*, 1995] and of seasonal cycles in $CO_2$ [*Hunt et al.*, 1996], these tests may not validate all aspects of transport relevant for $\delta(O_2/N_2)_{oc}$, which is unlike these tracers in having oceanic rather than continental sources. The ECMWF wind fields that are used in the TM2 model are known to have large uncertainties in the tropics [*Trenberth and Olson*, 1988]. Also, it is possible that the 1987 winds used for these simulations are not representative of climatological mean transports.

Deficiencies in our ability to simulate the low-latitude cycles may eventually be overcome with expanded oceanic and atmospheric observations and with improved understanding of atmospheric transport. Eventually, the $O_2/N_2$ observations have the potential to provide useful constraints on gas exchange at both low and high latitudes, although only the high-latitude constraints appear to be useful at the present time.

## 7. Optimized Average High-Latitude Gas-Exchange Velocities

Returning to the middle- and high-latitude optimizations, we have used these results to compute the temporally and

spatially averaged optimized gas-exchange velocity for the regions poleward of 31°N and 31°S in each hemisphere, as summarized in Table 5. In Table 5 we have also applied corrections for the bubble and covariance terms in (3) and (4), as described in Appendices B and C. These corrections are generally at the level of 5 to 15%, with the bubble and covariance effects partly compensating each other.

We have computed the overall uncertainty in these average exchange velocities based on the quadrature sum of errors associated with (1) imprecision in the harmonic fits to the atmospheric observations, (2) uncertainty in the $O_2$:C exchange coefficient associated with terrestrial exchanges (needed in Eq. (1)), (3) errors associated with the interpolation and regridding of the sparse oceanic $O_2$ data in constructing the $O_2$ maps, (4) uncertainty in the $N_2$ flux fields, (5) uncertainty in atmospheric transport, and (6) uncertainty in bubble and covariance effects. Estimates of the individual contributions to the uncertainty are summarized in Table 6. We allow for an uncertainty of the terrestrial exchange ratio $R_{O_2:C}$ of 1.10±0.05. We allow for uncertainty associated with sparse oceanic $O_2$ observations based on the sensitivity to changes brought about by the temperature-based scaling (see Appendix A and Figure 6). The uncertainty due to $N_2$ fluxes is based on an assumed ±20% uncertainty in the seasonally integrated net air-sea heat fluxes in the northern hemisphere and ±40% in the southern hemisphere. We allow for uncertainty in atmospheric transport at the ±20% level for the gas-exchange optimizations north of 31°N and for uncertainty at the ±30% level south of 31°S. The uncertainties are larger in the southern hemisphere because the analyzed fields there are based on fewer meteorological observations and have larger errors when compared to observations [*Trenberth and Olson*, 1988]. The basis for the estimated uncertainties in the bubble and covariance effects are discussed in Appendices B and C. The estimated uncertainties are only very rough estimates of probable error.

We have repeated the optimization calculations for the regions poleward of 31°N and 31°S starting with the $O_2$ fluxes computed using the alternative gas-exchange formulations based on the Liss and Merlivat formulation and on a constant gas-exchange velocity (see Table 3). The spatially and temporally averaged gas-exchange velocities that result after optimization are again given in Table 5. Starting with a constant gas-exchange velocity yields averages for the regions poleward of 31° that are smaller by about 20% in the northern hemisphere and 2% in the southern hemisphere. Seasonal variations in wind speed are much larger in the northern hemisphere, and this may account for the greater sensitivity to the wind speed formulation in this hemisphere. These results suggest that while the $O_2$ mass balance method clearly provides a strong constraint on the annual-average gas-exchange velocity, this

**Table 5.** Average Exchange Velocities and Corrections for Northern and Southern Regions

| | Northern Hemisphere 31°N to Pole | | | Southern Hemisphere 31°S to Pole | | |
|---|---|---|---|---|---|---|
| Gas Exchange Formulation[a] | W | LM | C | W | LM | C |
| Average gas-exchange velocity before optimization, cm/hr | 22.1 | 10.5 | 21.2 | 25.2 | 11.9 | 21.2 |
| Average Schmidt number (*Sc*) | 930 | 930 | 930 | 1180 | 1180 | 1180 |
| Average wind speed, m/s | 7.61 | 7.61 | 7.61 | 8.82 | 8.82 | 8.82 |
| Optimization factor | 1.15 | 2.47 | 0.96 | 1.23 | 2.46 | 1.44 |
| Correction factor for bubble effects | 0.90 | 0.90 | 0.90 | 0.90 | 0.90 | 0.90 |
| Correction factor for covariance effects | 1.05 | 1.05 | 1.05 | 1.05 | 1.05 | 1.05 |
| Average gas-exchange velocity after optimization and corrections, cm/hr | 24.0 | 24.6 | 19.1 | 29.3 | 29.8 | 28.8 |
| Average gas exchange velocity after optimizations and corrections scaled to $Sc = 600$,[b] cm/hr | 29.9 | 30.6 | 23.8 | 41.0 | 41.7 | 40.4 |

[a]W, *Wanninkhof* [1992]; LM, *Liss and Merlivat* [1986]; C, constant. See text.
[b]Assumes exchange velocity proportional to $Sc^{-1/2}$.

**Table 6.** Estimated Errors in Optimized Exchange Velocities

| Source of Error | Northern Hemisphere 31°N to Pole, % | Southern Hemisphere 31°S to Pole, % |
|---|---|---|
| Least squares fit optimization | ±4 | ±5 |
| Terrestrial $O_2$:C ratio | ±5 | ±0.4 |
| Due to oceanic data sparseness | ±10 | ±25 |
| Due to uncertainty in $N_2$ flux fields | ±3 | ±7 |
| Uncertainty in atmospheric transport | ±20 | ±30 |
| Bubble effects | ±10 | ±10 |
| Covariance effects | ±5 | ±5 |
| Quadrature sum of all errors | ±26 | ±42 |

constraint is also somewhat sensitive to seasonal variations in gas exchange, especially in the northern hemisphere where these seasonal variations may be quite significant.

To evaluate the sensitivity of the optimized average gas-exchange velocities to the initial wind speed data, we have repeated the entire simulation/optimization procedure starting with monthly wind speed atlas of *Wright* [1988] based on Comprehensive Ocean-Atmosphere Data Set (COADS) instead of the ECMWF winds in the Wanninkhof formula. Regions with missing wind speed values were assigned values by using a Laplacian interpolation scheme. Although these wind fields differ significantly from the ECMWF winds, especially in the southern hemisphere, the resulting optimized average gas-exchange velocities differed by less than 4% in both hemispheres from the values given in Table 5. This demonstrates that our reported optimized average gas-exchange velocities are not sensitive to the initial choice of the wind speed climatology.

It is important to emphasize, however, that the rescaling factors themselves, which may be helpful in evaluating the applicability of the different gas-exchange formulations, are critically dependent on the wind speed climatology. We have compared the monthly ECMWF 10-m wind speed climatology used in our computations with an alternative climatology derived from the ERS scatterometer data from August 1991 to April 1996 (J. Boutin, personal communication, 1997). Generally, the differences were small, suggesting that errors in the wind climatology are not a major source of uncertainty in our analyses. Another possible limitation is that the rescaling factors that we compute for the simulations with the Liss and Merlivat relation do not account for possible enhancement in the gas exchange due to wind speed variance within the monthly averaging periods. For the simulations with the Wanninkhof formulation, this variance was explicity accounted for in the gas-exchange formulation, where a Rayleigh distribution was used to approximate the wind speed distribution [*Wanninkhof*, 1992]. If the same wind speed distribution is assumed with the Liss and Merlivat formulation, the monthly average gas-exchange velocities for the relevant regions are increased by between 10 and 20%. The enhancement due to wind speed variance is in the right direction but falls far short of the magnitude needed to bring the simulations using the Liss and Merlivat formulation into agreement with the observations.

## 8. Discussion and Summary

We have presented observations of the oceanic component of the seasonal cycle in the atmospheric $O_2/N_2$ ratio that document systematic variations in this cycle with latitude and altitude. We have shown that an atmospheric transport model driven by air-sea $O_2$ and $N_2$ exchanges is successful at simulating many features of the observed seasonal variations in the $O_2/N_2$ ratio. The model is based on $O_2$ fluxes derived from a monthly climatology of the $O_2$ anomaly in surface waters and $N_2$ fluxes based on the net air-sea heat flux. By optimizing the model, we have derived estimates of the average gas-exchange velocity for the regions poleward of 31°N and 31°S. The approach essentially invokes the mass balance of $O_2$ between the atmosphere and oceans on seasonal timescales.

Our average gas-exchange velocities agree within the uncertainties with gas-exchange velocities derived for these regions using the *Wanninkhof* [1992] relation and the ECMWF winds. Insofar as the Wanninkhof relation was scaled to match the global radiocarbon constraints, our results support the magnitude of the average gas-exchange velocities implied by the distribution of radiocarbon between the atmosphere and the oceans. We estimate that the $O_2$-derived average gas-exchange velocity for the northern hemisphere has an uncertainty of around 25%, which is comparable to the uncertainties in large-scale velocities derived using the radiocarbon constraints. Like

the radiocarbon-derived exchange velocities, the $O_2$-derived gas-exchange velocities are about twice as large as those implied by the *Liss and Merlivat* [1986] relation. The apparent inadequacy of the Liss and Merlivat relation was also commented on recently by *Suntharalingam and Sarmiento* [1995] who found that larger exchange velocities are needed to reconcile observed and modeled $N_2O$ distributions in the oceans.

These results show that air-sea gas exchange in the open ocean is enhanced by processes that were not systematically accounted for in the experiments on wind/wave facilities and lakes used to derive the Liss and Merlivat relation. Furthermore, this enhancement is required for at least several gases besides just $CO_2$, so it cannot be caused primarily by hydration reactions of $CO_2$. The results are not necessarily incompatible, however, with local studies that have found evidence for smaller rates of gas exchange [*Watson et al.*, 1991; *Emerson et al.*, 1991; *Spitzer and Jenkins*, 1989], because the enhancement may not be uniform in the ocean.

We emphasize that the constraints on gas exchange poleward of 31° in each hemisphere are essentially independent of each other. The northern hemisphere constraint is the more powerful of the two because the data density of dissolved oceanic $O_2$ measurements is greater and because atmospheric transports are better known in the north. We have attempted to correct for deficiencies in ocean data coverage by using a temperature-based rescaling, although this procedure is clearly not entirely satisfactory. In time, this deficiency will diminish as additional oceanic $O_2$ measurements become available. Nevertheless, the fact that we arrive at similar conclusions in both hemispheres suggests that our results are not heavily influenced by data sparseness even at the present time.

In contrast to the situation at higher latitudes, the $O_2$ mass balance constraint on the gas-exchange velocity between 31°S and 31°N is very weak and is certainly not incompatible with gas-exchange velocities of the magnitude expected from either the Liss and Merlivat or Wanninkhof relations. Lower gas-exchange velocities in low latitudes relative to high latitudes would increase the global uptake of $CO_2$ computed using observations of the $CO_2$ partial pressure difference between the water and the air [*Tans et al.*, 1990; *Takahashi et al.*, 1997] because low latitudes are a region of net $CO_2$ outgassing that partially offsets the net $CO_2$ uptake at higher latitudes. The relative magnitude of the gas exchange between low and high latitudes thus remains an important question requiring further research.

Two aspects of the comparison between the gas-exchange velocities computed with mass balance of radiocarbon and $O_2$ deserve further comment. First, because the approaches are based on different gases, the comparison depends on the scaling rule used to relate gas-exchange velocities from one gas to another. The formulas we have adopted assume that the exchange velocity scales proportionally to $Sc^{-1/2}$ [*Wanninkhof*, 1992], which yields a ratio $K_{O_2}/K_{CO_2}$ of 1.1 with only a slight dependence on temperature. The Schmidt number exponent (here taken as $-\frac{1}{2}$) can vary depending on the type and character of surface turbulence, although this has little impact on $K_{O_2}/K_{CO_2}$ because the Schmidt numbers of $O_2$ and $CO_2$ are similar. Nevertheless, the ratio $K_{O_2}/K_{CO_2}$ could be significantly smaller than 1.1 if chemical enhancement of $CO_2$ exchange is important or significantly larger than 1.1 if large bubbles, which preferentially enhance the exchange velocities of gases with lower solubilities (like $O_2$), contribute significantly to gas exchange [Merlivat and Memery, 1983; *Keeling*, 1993].

In fact, we can derive an empirical estimate of $K_{O_2}/K_{CO_2}$ by combining our results for $O_2$ with the exchange velocities for $CO_2$ based on the radiocarbon mass balance constraints. Here we take the value for $K_{O_2}$ from the optimized and corrected gas-exchange velocities in Table 5 and the value for $K_{CO_2}$ based on computing the averages over the appropriate regions using the *Wanninkhof* [1992] gas-exchange formulation with ECMWF winds and using the Schmidt number formulation for $CO_2$ from *Wanninhof* [1992]. We thus derive a ratio of 1.2±0.4 for the northern hemisphere and 1.3±0.6 for the southern hemisphere, where we allow for uncertainty in $K_{O_2}$ from Table 6 and allow for 25% uncertainty in the computed values of $K_{CO_2}$ [*Wanninkhof*, 1992]. In effect, the comparison confirms that the exchange velocities of $O_2$ and $CO_2$ are approximately equal, but there is still room for possible modest enhancement of $O_2$ exchange by bubbles or $CO_2$ exchange by hydration given the uncertainties.

Second, the comparison between the gas-exchange velocities computed with mass balance of radiocarbon and $O_2$ is complicated because the constraints apply to different oceanic regions. The radiocarbon mass balance method provides constraints on the gas-exchange velocity for different isolated oceans (e.g., Atlantic versus Pacific) and for the globe as a whole, but it does not independently constrain the gas exchange in different latitude zones because of complications involving meridional water mass transport and mixing. In contrast, the $O_2$ mass balance method provides a constraint on gas exchange for broad latitude bands such as those used in this study, but it does not constrain gas exchange in the different oceans because of zonal atmospheric mixing. To compare the methods, we have implicitly adopted the spatial patterns of gas exchange determined by the ECMWF winds and the *Wanninkhof* [1992] gas-exchange relation, which predict that the average $K_{O_2}$ north of 31°N is 1.04 times the global average, while the average $K_{O_2}$ south of 31°S is 1.19 times the global average. The pattern depends on the variations in temperature and wind speed, which tend to produce compensating effects on the exchange velocity. This near constancy in the large-scale averages is effectively a postulate based on reasonable assumptions, but it has not yet been tested. Furthermore, wind speed alone is known to be an insufficient basis for predicting variations in gas

exchange caused by wind and wave forcing [*Wanninkhof*, 1992]. In principle, the spatial pattern in gas-exchange velocity could be determined using the Rn evasion method [*Peng et al.*, 1979; *Roether and Kromer*, 1984; *Kholouiski* 1995], but this will require much better spatial and temporal coverage than is currently available. Until we have a better understanding of the spatial variations in gas exchange, the comparison between the radiocarbon and $O_2$ methods must be viewed with caution.

We conclude by showing in Figure 8 the spatial patterns of the amplitude and phasing of the oceanic component of the $O_2/N_2$ seasonal variations predicted by the optimized gas-exchange model over the full surface of the earth. Larger amplitudes and earlier phasing are predicted over the

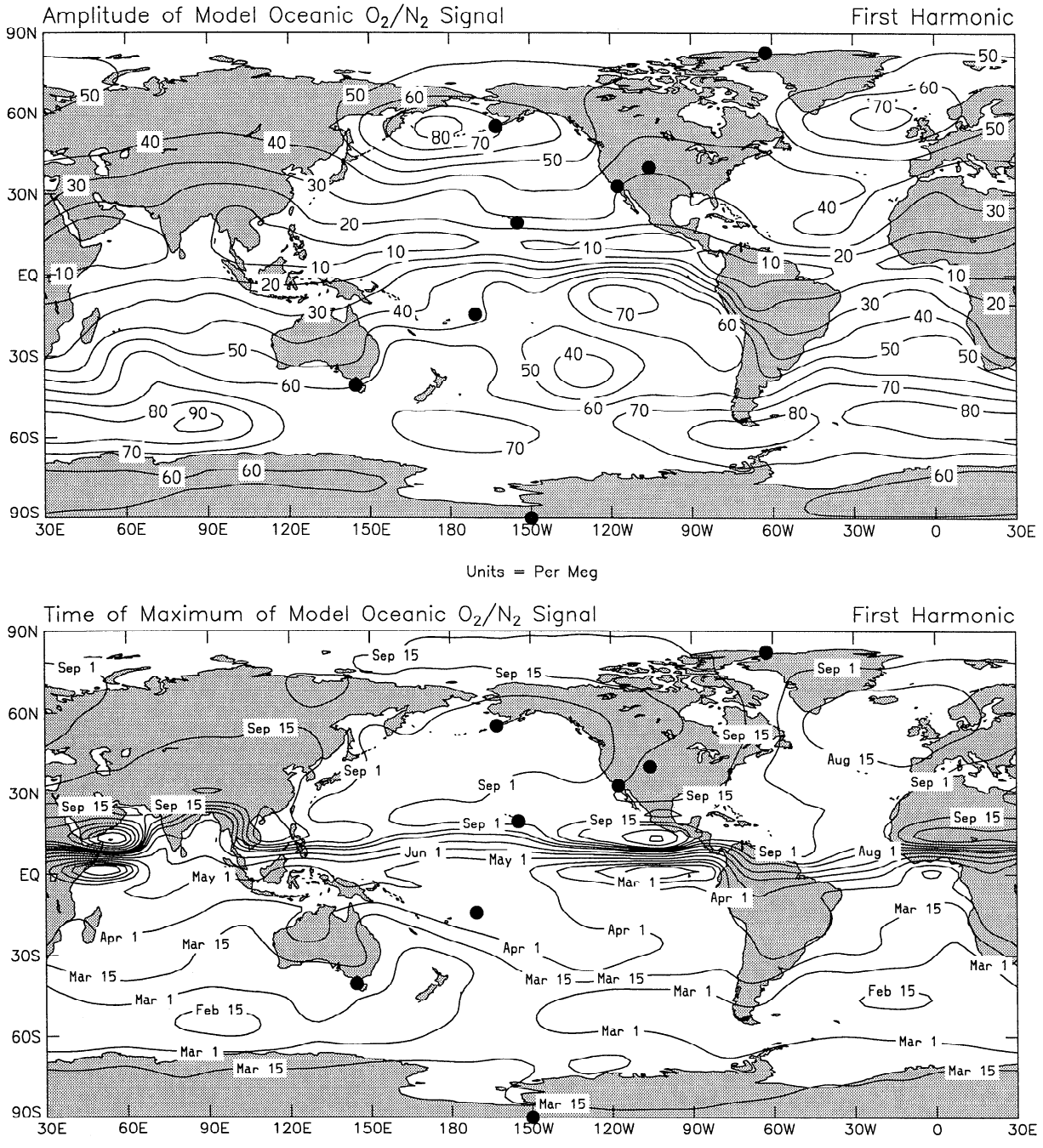


Figure 8. Modeled peak-to-peak amplitude and phasing of the first harmonic (fundamental) of the atmospheric $O_2/N_2$ annual cycles at the surface arising from air-sea $O_2$ and $N_2$ exchanges. Results are shown of the optimized model using Wanninkhof/ECMWF exchange velocities rescaled by the optimization factors from Table 5 for regions poleward of 31°N and 31°S. Sampling stations are shown as bold circles, with Mauna Loa and Kumukahi indicated by a single circle.

oceans relative to the continents in the northern hemisphere. The largest amplitudes in the northern hemisphere are predicted in the North Pacific, centered on the Aleutian Islands. The predicted Atlantic maximum is centered between Scotland and Iceland. Globally, the largest amplitudes are predicted in a band along 55° to 60°S in the Southern Ocean, and the smallest amplitudes are predicted over tropical South America and Africa. The equatorial minimum in the amplitude is predicted to coincide with the zone of most rapid north-south change in phase. This "node" extends along 10°N in the Pacific and along the equator in the Atlantic. These model predictions may be tested if more extensive observations become available.

## Appendix A: Scaling the Oxygen Anomaly Maps Using Temperature

The oxygen anomaly maps of *Najjar and Keeling* [1997] were modified using sea surface temperature (SST) analyses as follows. The monthly SST analyses of *Shea et al.* [1992] were averaged into 12° latitude bands for each of the major ocean basins. We then computed the fundamental annual harmonic amplitude of these averaged data. We then computed another set of temperature analyses using only temperature observations where concurrent $O_2$ anomaly values were available and by applying the same filtering and smoothing techniques as for the $O_2$ anomaly data [*Najjar and Keeling*, 1997]. Again, we computed the fundamental annual harmonics based on this reduced temperature data set. We then derived a rescaling factor $S$, based on the ratio of the *Shea et al.* [1992] (fundamental harmonic) amplitude to the amplitude of the reduced data set. By design, the scale factor $S$ varies between ocean basins but is constant for each 12° latitude band within each basin. We multiplied the oxygen anomaly by $S$ at every grid point after subtracting the annual mean oxygen anomaly at each point. The final, scaled oxygen anomaly maps were obtained after adding back the annual mean oxygen anomaly from each point. For the purpose of error analysis, we allow for uncertainty in the scaled maps by letting $S$ vary over the range of $S \pm (S - 1)$.

## Appendix B: Corrections for Bubble Effects

Our estimates of the air-sea $O_2$ flux neglect the bubble term in (3). The steady state $O_2$ anomaly $\Delta[O_2]_{bub}$ is expected to increase with wind speed and wave-induced turbulence [*Keeling*, 1993], and thus we generally expect $\Delta[O_2]_{bub}$ to be larger in winter, when $\Delta[O_2]$ is minimum than in summer when $\Delta[O_2]$ is maximum. This cycle in $\Delta[O_2]_{bub}$ therefore contributes to additional seasonal net ingassing and outgassing of $O_2$ not accounted for by the cycle in $\Delta[O_2]$ alone. The anomaly $\Delta[O_2]_{bub}$ is produced both by small bubbles, which collapse totally by gas dissolution, and larger bubbles, which exchange gases as they are subducted and then rise back to the surface.

Although several models of bubble effects on gas exchange have been proposed [*Thorpe*, 1984; *Spitzer and Jenkins*, 1989; *Wallace and Wirick*, 1992; *Farmer et al.*, 1993; *Schudlich and Emerson*, 1996], none is yet capable of accounting for the full spectrum of observed phenomena. Here we rely instead on direct estimates of the bubble effects based on measurements of inert gases, including He, Ne, Ar, and $N_2$. We focus here on the seasonal variations in $\Delta[O_2]_{bub}$ because the annual-mean values of $\Delta[O_2]_{bub}$ will mainly influence the annual-mean $O_2$ fluxes, which we have shown do not significantly impact the seasonal cycles in the atmospheric $O_2/N_2$ ratio.

Summertime bubble effects are constrained by local studies off Bermuda (32°N), Station Papa (50°N), and off Hawaii (24°N) [*Craig and Hayward*, 1987; *Spitzer and Jenkins*, 1989; *Emerson*, 1987; *Emerson et al.*, 1991; *Schudlich and Emerson*, 1996]. These studies consistently indicate that around 15 to 30% of the summertime supersaturation in $O_2$ is induced by bubbles, corresponding to $O_2$ saturation anomalies of the order of 1%, compared to typical total summertime anomalies at middle latitudes of around of 3 to 6%.

To constrain wintertime bubble effects at higher latitudes, we rely on observations of helium in North Atlantic Deep Water (NADW), which forms in the Labrador and Greenland Seas in wintertime and spreads laterally throughout the deep Atlantic. Helium concentrations in NADW are observed to be supersaturated by between 4 and 6% [*Bieri et al.*, 1968, *Weiss*, 1971; *Jenkins and Clarke*, 1976], with average values closer to 4% in the North Atlantic and closer to 6% in the South Atlantic [*Jenkins and Clarke*, 1976]. The northern values presumably reflect atmospheric helium present when the water was last in contact with the atmosphere because here the contribution from radiogenic helium from hydrothermal systems is unimportant [*Jenkins and Clarke*, 1976].

The northern helium anomalies could reflect several surface processes including temperature changes after equilibration, barometric pressure anomalies, and bubble effects. Wintertime barometric pressure in the Greenland and Labrador Seas alone would induce undersaturation (relative to 1 atm pressure) of approximately 0.7% [*Peixoto and Oort*, 1992, Figure 7.1]. Thus, assuming the temperature effects are negligible because the helium solubility is virtually independent of temperature, we estimate a net bubble-induced helium supersaturation of the order of 5%.

Assuming that small bubble processes dominate and a steady state supersaturation is achieved, the percent bubble-induced supersaturation should scale in proportion to $\gamma = \alpha^{-1} D^{-1/2}$ [*Fuchs et al.*, 1987; *Keeling*, 1993], where $\alpha$ is the solubility and $D$ is the diffusivity. Using solubility data summarized by *Weiss* [1970, 1971] and diffusivity (actually Schmidt number) data summarized by *Wanninkhof* [1992], we find $\gamma_{O_2}/\gamma_{He} = 0.46$, suggesting that $\Delta[O_2]_{bub}$ should equal roughly 2.3% of saturation in the high-latitude wintertime North Atlantic.

A very similar estimate is achieved using the Ne saturation anomalies in the deep Atlantic [*Bieri et al.*, 1968; *Weiss* 1970; *Jenkins* 1974], although the neon saturation anomaly is more sensitive to temperature changes after equilibration because of the larger temperature dependence of the neon solubility. Thus the helium-based estimate is probably the more reliable of the two. In any case, deep Atlantic neon and helium data both are consistent with values of $\Delta[O_2]_{bub}$ of around 2% of saturation in the wintertime North Atlantic. This estimate applies to a region of rather extreme wintertime forcing and can thus probably serve as an upper bound for the average wintertime bubble effect at middle and high latitudes.

In middle and high latitudes of the northern hemisphere, the peak-to-peak seasonal amplitude in $\Delta[O_2]$ [*Najjar and Keeling*, 1997] is typically around 5% to 10% of the saturation concentration. In comparison, the above estimates of bubble phenomenology suggest that $\Delta[O_2]_{bub}$ varies with opposite phase between about 1% of the saturation concentration in summer to a maximum of 2% in winter, with a probable seasonal variation not greater than 1%. These considerations suggest that the bubble term in (3) on average increases the seasonal outgassing and ingassing of $O_2$ by at most 20% relative to the first term in (3). To correct our "optimized" gas-exchange velocities in the northern hemisphere for bubble effects, we thus need to reduce their magnitude by between 0 and 20%. In the middle and high latitudes of the southern hemisphere, the peak-to-peak amplitude in $\Delta[O_2]$ is typically around 3 to 10% of the saturation concentration (after allowing for the temperature-based scaling), while the seasonal variations in $\Delta[O_2]_{bub}$ are probably comparable or smaller than in the northern hemisphere because seasonal variations in wind speed are smaller [*Wright*, 1988]. Since additional information is lacking, we assume the bubble corrections are comparable in both hemispheres.

These estimates do not fully account for the effects of large bubbles, which were neglected in some of the local studies cited above and were neglected in the formula used above for scaling He anomalies to $O_2$ anomalies. The theoretical study of *Keeling* [1993] suggests that although large bubbles contribute significantly to $K_{O_2}$, their contribution globally to $\Delta[O_2]_{bub}$ is probably not larger than 0.5% of the saturation concentration. The seasonal variations would necessarily be smaller than 0.5%, suggesting that the large bubble contribution to $\Delta[O_2]_{bub}$ is probably insignificant in the present context. On the other hand, the *Keeling* [1993] model is not well constrained, and the *Schudlich and Emerson* [1996] results raise the possibility of more significant large bubble effects, especially in the winter. Here we will neglect the large-bubble contribution, although more work is clearly needed to quantify these effects.

In summary, we estimate that allowing for bubble phenomenology reduces the required gas-exchange velocities by the $O_2$ mass balance method by between 0 and 20%. We emphasize, however, that these estimates are rather poorly constrained and that further studies of bubble phenomenology are clearly needed, especially at middle and high latitudes in winter.

## Appendix C: Correction For Covariance Effects

Our calculations of the air-sea $O_2$ flux also neglect the covariance term in (4). This term is not easily evaluated from observational data but can be estimated from upper ocean models. Here we consider two such models, one developed for Station Papa in the North Pacific [*Archer et al.*, 1993] and the other for the Bermuda Atlantic Time Series (BATS) station in the North Atlantic [*Doney et al.*, 1996; *Doney*, 1996]. Both models incorporate a one-dimensional representation of the physics of the mixed layer and a simple ecosystem model. Both models are capable of resolving mixed layer dynamics and the response of gas exchange to forcing by synoptic weather events. The BATS model incorporates an ecosystem model that responds to synoptic forcing, while the Station Papa model uses a fixed rate of biological production of $O_2$ when nutrients are not limiting.

Results from the BATS model are illustrated in Figure 9. The gas-exchange velocity is shown to vary by a factor of 10 or more on timescales of a few days or less. These fluctuations result from the instantaneous response of the gas-exchange velocity to fluctuations in wind speed associated with the passage of synoptic weather systems. In contrast, the $O_2$ anomaly exhibits distinct diurnal variations associated with variations in net photosynthesis, respiration, heating, and cooling. Aside from these diurnal variations, the $O_2$ anomaly mostly varies on a timescale of a few days or longer. These fluctuations result from variations in the entrainment of deeper water, variations in photosynthesis and respiration, changes in surface temperature, and air-sea gas exchange. These processes produce prompt variations in the time derivative of the $O_2$ anomaly, with the $O_2$ anomaly generally responding to the time integral of the forcing. The fluctuations in $O_2$ anomaly are therefore effectively subjected to a low-pass filter with a cut-off frequency approximately equal to the timescale for the mixed layer $O_2$ anomaly to equilibrate with the overlying air. This time constant is typically between 1 and 4 weeks depending on the mixed layer depth and the mean gas-exchange coefficient, and thus the $O_2$ anomaly generally tends to vary more slowly than the gas-exchange velocity.

For both the Station Papa and BATS models, we compute the local seasonal net outgassing (SNO) of $O_2$ according to

$$\mathrm{SNO} = \frac{1}{2}\int_{\mathrm{year}} \left| F_{O_2} - \langle F_{O_2} \rangle \right| dt \qquad (5)$$

where $\langle F_{O_2} \rangle$ is the annual-net influx or efflux of $O_2$. SNO is the locally balanced seasonal net efflux of $O_2$ and is a

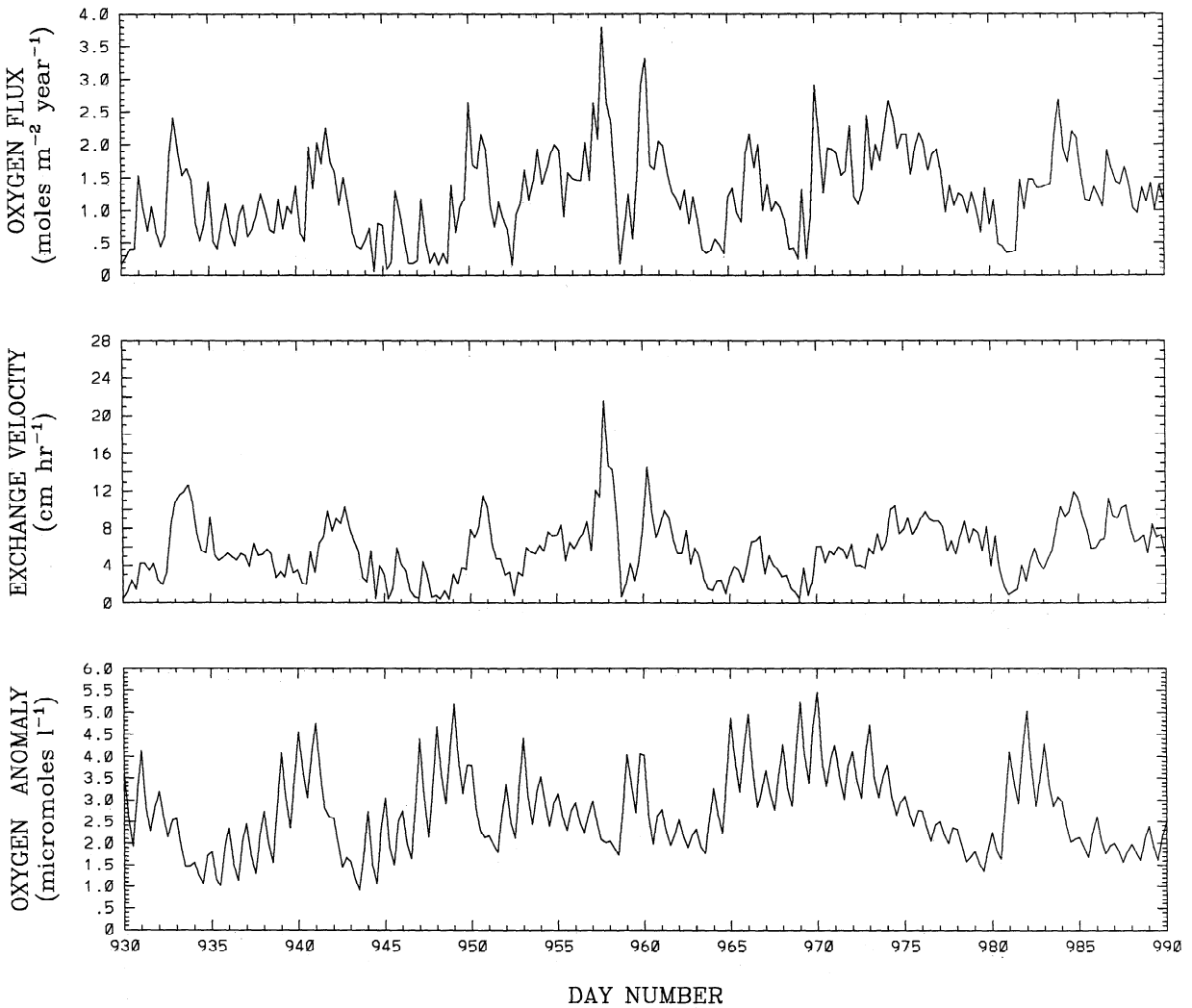


Figure 9. Simulated variations in air-sea oxygen flux, exchange velocity, and oxygen anomaly at the BATS station near Bermuda using the model of *Doney et al.* [1996].

useful measure of the fraction of the total yearly $O_2$ exchange that affects the seasonal cycle of $O_2/N_2$ in the atmosphere. We compute SNO using fully time-resolved variations in the gas-exchange velocity and $O_2$ anomaly from the models. We then compute the 31-day running averages of the gas-exchange velocity and $O_2$ anomaly and recompute SNO using these running averages. The relative differences between these versions of SNO are a measure of the importance of the short-term covariance term in (4).

For both models, we find that computing fluxes using time-averaged anomalies and exchange velocities leads to an overestimate of SNO. The degree of overestimation varies from year to year as a result of interannual variations in the physical forcing. Depending on the model year, we find that SNO is overestimated by 0 to 12% in the Papa model and by 0 to 4% in the BATS model. Although a variety of factors contribute, the dominant reason that SNO is overestimated in the models is that during periods of persistent high gas-exchange velocity the $O_2$ anomaly tends to be driven toward zero. Using the time-averaged $O_2$ anomaly instead of the actual anomaly therefore leads to an overestimate of the long-term average flux.

In any event, both models suggest that the covariance term is relatively small. Although additional studies may be desirable, we expect that this result is likely to be generally valid as it is an expected consequence of the separation in timescales between the synoptic forcing and the response of the $O_2$ anomaly, as discussed above. Our limited analysis thus suggests that by neglecting covariance effects, we overestimate seasonal ingassing and outgassing of $O_2$ by between 0 and 10% in the model. It follows that we need to increase the optimized gas-exchange velocities by between 0 and 10% to correct for the covariance effect. Note that the covariance correction is likely the same order of magnitude but is the opposite sign of the bubble correction.

**Acknowledgments.** The flask program at Scripps has been run by Elizabeth McEvoy, Andrew Manning, and Bill Paplawsky, who we thank for their expert services. We thank Niel Trivet,

Roger Francey, Russ Schnell, John Chin, Mark Winey, Taylor Ellis, Michael Bender, Pieter Tans, Chuck Yates, Jerry Painter, Steve Shertz, and staff at the Canadian Baseline Program, staff of the NOAA-CMDL program at Mauna Loa, Kumukahi, Samoa, and the south pole, staff of the National Weather Service at Cold Bay, and staff of the Cape Grim Station for collection of air samples. We thank Dave Erickson, Jim Elkins, and Bill Jenkins for valuable discussions. The draft was improved by insightful reviews by Steve Emerson and Andrew Watson. The $O_2/N_2$ and $CO_2$ analyses were supported by the National Science foundation under grant ATM-9309765 and the Environmental Protection Agency Global Change Research Program under IAG#DW49935603-01-2. The modeling and mapping work was supported by NASA under grant 2383-MDIS/BGE005. B. Stephens is supported by an NSF graduate fellowship. The National Center for Atmospheric Research is sponsored by the National Science Foundation.

## References

Archer, D., S. Emerson, and C.S. Wong, Numerical hindcasting of sea surface $pCO_2$ at Weathership Station Papa, *Prog. Oceanogr.*, *32*, 319-351, 1993.

Bender, M., J.T. Ellis, P.P. Tans, R.J. Francey and D.Lowe, Variability in the $O_2/N_2$ ratio of southern hemisphere air, 1991-1994: Implications for the carbon cycle, *Global Biogeochem. Cycles, 10*, 9-21, 1996.

Berger, R. and W.F. Libbey, Equilibration of atmospheric carbon dioxide with seawater: Possible enzymatic control of the rate, *Science, 164*, 1395-1397, 1969.

Bieri, R.H., M. Koide, and E.D. Goldberg, Noble gas contents of marine waters, *Earth Planet. Sci. Lett.,4,* 329-340, 1968.

Broecker, W.S. and T.-H. Peng, Gas exchange rates between air and sea, *Tellus, 26*, 21-35, 1974.

Broecker, W.S., T.-H. Peng, G. Ostlund and M. Stuiver, The distribution of bomb radiocarbon in the ocean, *J. Geophys. Res.*, *90*, 6953-6970, 1985.

Broecker, W.S., J.R. Ledwell, T. Takahashi, R. Weiss, L. Merlivat, L. Memery, T.-H. Peng, B. Jähne and K.O. Münnich, Isotopic versus micrometeorological ocean $CO_2$ fluxes: A serious conflict. *J. Geophys. Res. 91*, 10517-10527, 1986.

Craig, H. and T. Hayward, Oxygen supersaturation in the ocean: Biological versus physical contributions, *Science,235,* 199-202, 1987.

Doney, S.C., A synoptic atmospheric surface forcing data set and physical upper ocean model for the U.S. JGOFS Bermuda Atlantic Time-Series Study site, *J. Geophys. Res., 101*, 25615-25634, 1996.

Doney, S.C., D.M. Glover and R.G. Najjar, A new coupled one-dimensional biological-physical model for the upper ocean—Applications to the JGOFS Bermuda Atlantic Time Series Study (BATS) site, *Deep Sea Res., Part II, 43*, 591-624, 1996.

Emerson, S., Seasonal oxygen cycles and biological new production in surface waters of the subarctic pacific ocean, *J. Geophys. Res.*, *92*, 6535-6544, 1987.

Emerson, S., Enhanced transport of carbon dioxide during gas exchange, in *Air-Water Gas Transfer*, edited by B. Jähne and E.C. Monahan, AEON, Hanau, Germany, pp. 23-35, 1995.

Emerson, S., P. Quay, C. Stump, D. Wilbur and M. Knox, $O_2$, Ar, $N_2$, and $^{222}Rn$ in surface waters of the subarctic ocean: Net biological $O_2$ production, *Global Biogeochem. Cycles, 5*, 49-69, 1991.

Erickson, D.J.I., P.J. Rasch, P.P. Tans, P. Friedlingstein, P. Ciais, E. Maier-Reimer, K. Six, C.A. Fischer, and Walters, S., The seasonal cycle of atmospheric $CO_2$: A study based on the NCAR Community Climate Model (CCM2), *J. Geophys. Res.*, *101*, 15079-15097, 1996.

Farmer, D.W., C.L. McNeil, and B.D. Johnson, Evidence for the importance of bubbles in increasing air-sea gas flux, *Nature, 361*, 620-623, 1993.

Fuchs, G., W. Roether, P. Schlosser, Excess $^3He$ in the ocean surface layer, *J. Geophys. Res., 92*, 6559-6568, 1987.

Gibson, J. K., P. Kallberg, S. Uppala, A. Hernandez, A. Nomura, and E. Serrano, ECMWF Re-Analysis, Project Report Series: 1. ERA description, Eur. Cent. forMedium-Range Weather Forecasts, 72 pp., Reading, England, 1997.

Hasse, L., The sea surface temperature deviation and the heat flow at the air-sea interface, *Boundary Layer Meteorlogy, 1*, 368-379, 1971.

Heimann, M., The global atmospheric tracer model TM2,Tech. Rep. 9, pp.1-51, Dtsch. Klimarechenzentrum, Hamburg, Germany, 1995.

Heimann, M. and C.D. Keeling, A three-dimensional model of atmospheric $CO_2$ transport based on observed winds, 2, Model description and simulated tracer experiments,in *Aspects of Climate Variability in the Pacific and Western Americas, Geophys. Monogr., vol. 55*, editedby D.H. Peterson, AGU, Washington D. C., pp. 237-275, 1989.

Hunt, E.R., S.C. Piper, R. Nemani, C.D. Keeling, R.D. Otto and S.W. Running, Global net carbon exchange and intra-annual atmospheric $CO_2$ concentrations predicted by an ecosystem process model and three-dimensional atmospheric transport model, *Global Biogeochem. Cycles, 10*, 431-456, 1996.

Jähne, B., Zur Parameterisierung des Gasaustausches mit Hilfe von Laborexperimenten, Doctoral dissertation, 124 pp., Univ. of Heidelberg, Heidelberg, Germany, 1980.

Jenkins, W.J., Helium isotope and rare gas oceanology, Ph.D. thesis, 171pp.,McMaster Univ., Hamilton, Ontario Canada, 1974.

Jenkins, W.J. and W.B. Clarke, The distribution of $^3He$ in the western Atlantic Ocean, Deep Sea Res., *Oceanogr. Abstr. 23*, 481-494, 1976.

Jenkins, W.J., and J.C. Goldman, Seasonal oxygen cycling and primary production in the Sargasso Sea, *J. Mar. Res.*, 43, 465-491, 1985.

Keeling, R.F., Development of an interferometric oxygen analyzer for precise measurement of the atmospheric $O_2$ mole fraction, Ph.D. thesis, 178pp., Harvard University, Cambridge, Mass., 1988.

Keeling, R.F., On the role of large bubbles in air-sea gas exchange and supersaturation in the ocean, *J. Mar. Res., 51*, 237-271, 1993.

Keeling, R.F. and S.R. Shertz, Variations in atmospheric molecular oxygen at Mauna Loa, in *Climate Monitoring and Diagnostics Laboratory, No. 20, Summary Report 1991*, edited by E.E. Ferguson and R.M. Rosson, pp. 103-104, U.S. Dep. Comm. Boulder, 1992a.

Keeling, R.F. and S.R. Shertz, Seasonal and interannual variations in atmospheric oxygen and implications for the global carbon cycle, *Nature 358*, 723-727, 1992b.

Keeling, R.F., R.G. Najjar, M.L Bender and P.P. Tans, What atmospheric oxygen measurements can tell us about the global carbon cycle. *Global Biogeochem. Cycles, 7*, 37-67, 1993.

Keeling, R.F., S.C. Piper and M. Heimann, Global and hemispheric $CO_2$ sinks deduced from measurements of the atmospheric oxygen concentration, *Nature, 381*, 218-221, 1996.

Kholouiski, S.N., Radon-222 transfer coefficients in Atlantic and Pacific oceans. The influence of temperature and wind,

in *Air-Water Gas Transfer*, edited by B. Jähne and E.C. Monahan, pp. 713-722, AEON, Hanau, Germany, 1995.

Kurz, K.D., Zur Saisonalen Variation des Ozeanischen Kohlendioxidpartialdrucks, Ph.D. thesis, 107 pp., Max-Planck-Institut für Meteorologie, Hamburg, Germany, 1993.

Liss, P.S., and L. Merlivat, Air-sea gas exchange rates: Introduction and synthesis, in *The Role of Air-Sea Exchange in Geochemical Cycling*, edited by P. Buat-Menard, pp. 113-127, D. Reidel, Norwell, Mass., 1986.

Merlivat, L. and L Memery, Gas exchange across an air-water interface: Experimental results and modeling of bubble contribution to transfer, *J. Geophys. Res., 88*, 707-724, 1983.

Najjar, R.G. and R.F. Keeling, Analysis of the mean annual cycle of the dissolved oxygen anomaly in the world ocean. *J. Mar. Res., 55*, 117-151, 1997.

Oberhuber, J.M., An atlas based on the COADS set: The budgets of heat, buoyancy and turbulent kinetic energy at the surface of the global ocean, *Rep.15*, pp. 1-20, Max-Planck-Inst. für Meteorol., Hamburg, Germany, 1988.

Peixoto, J.P. and A.H. Oort, *Physics of Climate*, 520 pp., Am. Inst. for Phys., New York, 1992.

Peng, T.-H., T. Takahashi, and W.S. Broecker, Radon evasion rates in the Atlantic and Pacific oceans as determined during the GEOSECS program, *J. Geophys. Res. 84*, 2471-2486, 1979.

Ramonet, M., P. Monfray, $CO_2$ baseline concept in 3-D atmospheric transport models, *Tellus, Ser. B*, 48, 502-520, 1996.

Roether, W. and B. Kromer, Optimum application of the radon deficit method to obtain air-sea gas exchange rates, in *Gas Transfer at Water Surfaces*, edited by G.H.Jirka and W. Brutsaert, pp. 447-457, D. Reidel, Norwell,Mass., 1984.

Schudlich, R. and S. Emerson, Gas supersaturation in the surface ocean: The role of heat flux, gas exchange, and bubbles, *Deep Sea Res., Part II , 43*, 569-589, 1996.

Severinghaus, J.P., Studies of the terrestrial $O_2$ and carbon cycles in sand dune gases and in Biosphere 2, Ph.D. thesis, 148 pp., Columbia University, New York, 1995.

Shea, D.J., K.E. Trenberth, and R.W. Reynolds, A global monthly sea surface temperature climatology, *J. Clim., 5*, 987-1001, 1992.

Six, K. D., E. Maier-Reimer, Effects of plankton dynamics on seasonal carbon fluxes in an ocean general circulation model, *Global Biogeochem. Cycles, 10*, 559-583, 1996.

Spitzer, W.S. and W.J. Jenkins, Rates of vertical mixing, gas exchange and new production: estimates from seasonal gas cycles in the upper ocean near Bermuda. *J. Mar. Res., 47*, 169-196, 1989.

Suntharalingam, P., J.L. Sarmiento, Modeling global air-sea $N_2O$ fluxes, a sensitivity analysis of the gas-exchange formulation, in: *Air-Water Gas Transfer*, edited by B. Jähne and E.C. Monahan, pp. 843-853, Hanau:AEON Verlag & Studio, 1995.

Takahashi, T., R.A. Feely, R. Weiss, R.H. Wanninkhof, D.W. Chipman, S.C. Sutherland, and T.T. Takahashi, Global air-sea flux of $CO_2$: An estimate based on measurements of the air-sea $pCO_2$ difference, *Proc. Nat. Acad. Sci. U.S.A., 94*, 8292-8299,1997.

Tans, P.P., I.Y. Fung, and T. Takahashi, Observational constraints on the atmospheric $CO_2$ budget, *Science, 247*, 1431-1438, 1990.

Thorpe, S.A., The role of bubbles produced by breaking waves in super-saturating the near-surface ocean mixing layer with oxygen, *Ann. Geophys., 2*, 53-56, 1984.

Trenberth, K.E., and J.G. Olson, An evaluation and intercomparison of global analyses from the National Meteorological Center and the European Center for Medium-Range Weather Forecasts, *Bull. Am. Meteorol. Soc., 69*, 1047-1057, 1988.

Wallace D.W.R., and C.D. Wirick, Large air-sea fluxes associated with breaking waves, *Nature, 356*, 694-696, 1992.

Wanninkhof, R., Relation between wind speed and gas exchange over the ocean, *J. Geophys. Res., 97*, 7373-7382, 1992.

Watson, A.J., R.C. Upstill-Goddard, and P.C. Liss, Air-sea exchange in rough and stormy seas, measured by a dual tracer technique, *Nature, 349*, 145-147, 1991.

Weiss, R.F., The solubility of nitrogen, oxygen and argon in water and seawater, *Deep Sea Res., 17*, 721-735, 1970.

Weiss, R.F., Solubility of helium and neon in water and seawater, *J.Chem. Eng. Data, 16*, 235-241, 1971.

Wright, P., An atlas based on the 'COADS' data set: Fields of mean wind, cloudiness and humidity at the surface of the global ocean, Max-Planck-Instit. für Meteorol., Rep.14, Hamburg, 22pp., Germany, 1988.

D. Archer, Department of Geophysical Sciences, University of Chicago, 5724 Ellis Avenue, Chicago, IL 60637. (e-mail: archer@popeye.uchicago.edu)

S.C. Doney, Climate and Global Dynamics Division, National Center for Atmospheric Research, Boulder, CO 80307. (e-mail: doney@ncar.ucar.edu)

M. Heimann, Max-Planck-Institut für Meteorologie, Bundesstrasse 55, 3000 Hamburg, Germany. (e-mail: heimann@dkrz.de)

R.F. Keeling and B.B. Stephens, Scripps Institution of Oceanography, University of California, San Diego, La Jolla, CA 92093-0236. (e-mail: rkeeling@ucsd.edu; bbstephe@ucsd.edu)

R.G. Najjar, Department of Meteorology, Pennsylvania State University, 503 Walker Building, University Park, PA 16802-5013. (e-mail: najjar@essc.psu.edu)

(Received January 23, 1997; revised August 4, 1997; accepted August 14, 1997.)